2750 *Inorg. Chem.* **2010**, *49*, 2750–2764
DOI: 10.1021/ic902126a

Inorganic Chemistry
Article

Synthesis, Spectral, Structural, Second-Order Nonlinear Optical Properties and Theoretical Studies On New Organometallic Donor−Acceptor Substituted Nickel(II) and Copper(II) Unsymmetrical Schiff-Base Complexes

Alexander Trujillo,[†] Mauricio Fuentealba,[‡,§] David Carrillo,*[,†] Carolina Manzur,*[,†] Isabelle Ledoux-Rak,[∥] Jean-René Hamon,*[,⊥,⊗] and Jean-Yves Saillard*[,⊥,⊗]

[†]*Laboratorio de Química Inorgánica, Instituto de Química, Pontificia Universidad Católica de Valparaíso, Campus Curauma, Avenida Parque Sur 330, Valparaíso, Chile,* [‡]*Laboratorio de Crystalografía, Departamento de Física, Facultad de Ciencias Físicas y Matemáticas, Universidad de Chile, Av. Blanco Encalada 2008, Santiago, Chile,* [§]*Facultad de Ecología y Recursos Naturales, Universidad Andrés Bello, Avenida República 275, Santiago, Chile,* [∥]*Laboratoire de Photonique Quantique et Moléculaire, UMR 8537 CNRS-ENS Cachan, Institut d'Alembert, 61 Avenue du Président Wilson, 94235 Cachan Cedex, France,* [⊥]*UMR 6226 Sciences Chimiques de Rennes, CNRS-Université de Rennes 1, Campus de Beaulieu, 35042 Rennes-Cedex, France, and* [⊗]*Université Européenne de Bretagne, 5 Bd Laënnec, 35000 Rennes, France*

Received October 27, 2009

The synthesis, spectroscopic and structural characterization, linear and nonlinear optical properties, as well as the electrochemical behavior of a series of robust neutral binuclear M[Fc-C(O)CH═C(CH_3)N-X-N═CH-(2-O,5-R-C_6H_3)] (M = Ni (**4**), Cu (**5**), X = *o*-C_6H_4, R = H; M = Ni (**9**), X = CH_2CH_2, R = OH), and their corresponding ionic trinuclear [M{Fc-C(O)CH═C(CH_3)N-X-N═CH-(η^6-2-O,5-R-C_6H_3)RuCp*}][PF_6] (**6**, **7**, **10**), M[ONNO]-type unsymmetrical Salophen and salen complexes featuring ferrocenyl (Fc) donor and the mixed sandwich acceptor [Cp*Ru(η^6-salicylidene)]$^+$ as a push−pull moiety are reported in this paper (Fc = CpFe(η^5-C_5H_4); Cp = η^5-C_5H_5; Cp* = η^5-C_5Me_5). The single-crystal X-ray structure of the bimetallic iron−nickel derivative **4** indicates a bowed structure of the unsymmetrical Schiff base skeleton. The Ni(II) ion is tetracoordinated in a square planar environment, with two nitrogen atoms and two oxygen atoms as donors. The new metalloligand [Fc-C(O)CH═C(CH_3)N-(H)CH_2CH_2N═CH-(2,5-$(OH)_2C_6H_3$)] (**8**) obtained from the Schiff base condensation of 2,5-dihydroxobenzaldehyde with the half-unit precursor, Fc-C(O)CH═C(CH_3)N(H)$CH_2CH_2NH_2$ (**2**), is reported with its crystal structure showing partial delocalization of the heteroconjugated [O−C−C−C-N] frameworks with a dihedral angle between the respective planes of 60.76°. Second order nonlinear optical (NLO) measurements were achieved using the Harmonic Light Scattering technique to probe the role of the M[ONNO] chromophores and of the π-complexation of the salicylidene ring in the nonlinearity. All the complexes exhibit a second-order nonlinear response increasing with the nuclearity, the hyperpolarizability (β) value of the trinuclear complex **10** being 1.5 time larger than that of the metalloligand **8** ($\beta = 155 \times 10^{-30}$ esu). A rationalization of the structural, electronic, and redox properties of the title compounds is provided, based on a theoretical investigation at the density functional theory (DFT) level. Their UV−visible spectra has been assigned with the help of time-dependent (TD) DFT calculations. They are dominated by LMCT, MLCT, and $\pi-\pi^*$ transitions.

Introduction

In the past decade there has been a growing interest in the design and construction of new molecular materials displaying second-order nonlinear optical (NLO) properties because of their potential applications in emerging optoelectronic and photonic technologies.[1,2] Molecules with high NLO responses (molecular hyperpolarizability, β) must possess strong electronic transitions of low energy and strong variations of the dipole moment during the electronic excitation.[3] These properties can be accomplished by compounds with a push−pull D-π-A type structure, containing both an electron donor group (D) and an electron acceptor group (A)

*To whom correspondence should be addressed. E-mail: david.carrillo@ucv.cl (D.C.), cmanzur@ucv.cl (C.M.), jean-rene.hamon@univ-rennes1.fr (J.-R.H.), saillard@univ-rennes1.fr (J.-Y.S.).

(1) (a) Goovaerts, E.; Wenseleers, W. E.; Garcia, M. H.; Cross, G. H. Nonlinear Optical Materials. In *Handbook of Advanced Electronic and Photonic Materials and Devices*; Nalwa, H. S., Ed.; Academic Press: New York, 2001; Vol. 9, p 127. (b) *Handbook of Optics IV, Fiber Optics & Nonlinear Optics* 2nd ed.; Bass, M., Enoch, J. M., Stryland, E. W. V., Wolfe, W. L., Eds.; McGraw-Hill: New York, 2001. (c) *Nonlinear optical properties of matter: From molecules to condensed phases*; Papadopoulos, M. G., Sadlej, A. J., Leszczynski, J., Eds.; Springer: India, 2006.

 Published on Web 02/10/2010

Chart 1

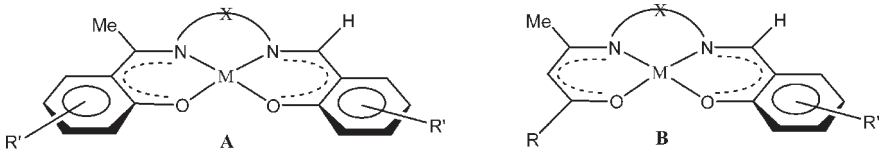

X= alkyl-chain or 1,2-phenylene.
R,R'= Donor or acceptor groups.

linked through a delocalized π system, which provides the polarizable electrons. In this regard, organic molecules with extensive π-delocalization have been the focus of the most intense activity because of their ultrafast NLO responses, good processability as thin-film devices, and enhanced nonresonant NLO responses.[4] More recently, the introduction of a metal center as a donor or acceptor subunit has led to the development of new second-order NLO materials based on organotransition metal complexes owing to the unique structural, electronic and optical properties associated with organometallic[5−7] and coordination compounds.[7−9] In this latter family, N_2O_2 Schiff base complexes (Chart 1, type **A**) in which ligands are derived from salicylaldehyde and diamines (generically coined as salen or salophen)[10] have appeared to be a promising class of efficient chromophores exhibiting potentially large NLO responses,[7a,11] and are currently attracting considerable interest.[12−15] They are particularly interesting because (i) of their preparative accessibility and the ease with which the salen-type structure can be derivatized, (ii) of their thermal stability, (iii) of the active role, strategic position, and nature (closed-shell vs open-shell)[16] of the metal ion which is a constituent of the polarizable bridge in the D-π-A structure, and (iv) of the presence of charge transfer (CT) transitions at low energies.[7a,11] In such compounds, metal complexation leads to formation of geometrically constrained acentric, generally planar structures that always involves an enhancement of optical nonlinearity of the Schiff base complex compared to that of its related free ligands. Note that in all the aforementioned NLO studies on salen- and bis(salicylaldiminato)-based complexes, including that recently reported with unsymmetrical Schiff bases (Chart 1, type **B**) of S-methylisothiosemicarbazide,[12b] organic groups have always been used to structurally and electronically modify the properties of the donor−acceptor Schiff base frameworks.

Furthermore, the electron-donating and -accepting capabilities of organoligand−metal fragments have been successfully applied to design and develop new highly efficient dipolar chromophores to achieve high second-order NLO responses.[1a,5−7] For instance, the attractive NLO properties of ferrocene-based complexes are coupled with good thermal and photochemical stability,[17] excellent donor capability,[18]

(2) (a) Zyss, J. *Molecular Nonlinear Optics: Materials, Physics and Devices*; Academic Press: Boston, 1994. (b) Prasad, P. N.; Williams, D. J. *Nonlinear Optical Effects In Molecules and Polymers*; Wiley & Sons: New York, 1991. (c) *Materials for Nonlinear Optics: Chemical Perspectives*; Marder, S. R., Sohn, J. E., Stucky, G. D., Eds.; ACS Symposium Series 455; American Chemical Society: Washington, DC, 1991. (d) *Optical Nonlinearities in Chemistry*; Burland, D. M., Ed.; *Chem. Rev*. **1994**, *94*, 1. (e) Delaire, J. A.; Nakatani, K. *Chem. Rev*. **2000**, *100*, 1817. (f) Verbiest, T.; Houbrechts, S.; Kauranen, M.; Clays, K.; Persoons, A. *J. Mater. Chem*. **1997**, *7*, 2175.

(3) (a) Cheng, L. T.; Tam, W.; Stevenson, S. H.; Meredith, G. R.; Rikken, G.; Marder, S. R. *J. Phys. Chem*. **1991**, *95*, 10631. (b) Cheng, L. T.; Tam, W.; Marder, S. R.; Stirgman, A. E.; Rikken, G.; Sprangler, C. W. *J. Phys. Chem*. **1991**, *95*, 10643.

(4) (a) *Nonlinear Optical Properties of Organic Molecules and Crystals*; Chemla, D. S., Zyss, J., Eds.; Academic Press: Orlando, 1987; Vols. *1 and 2*. (b) *Nonlinear Optics of Organic Molecules and Polymers*; Nalwa, H. S., Miyata, S., Eds.; CRC Press: New York, 1997. (c) *Organic Molecules for Nonlinear Optics and Photonics*; Messier, J., Kajzar, F., Prasad, P., Eds.; Kluwer Academic Publishers: Dordrecht, The Netherlands, 1991. (d) *Organic Materials for Nonlinear Optics II*; Hann, R. A., Bloor, D., Eds.; Royal Society of Chemistry: London, 1991. (e) Kuzyk, M. G.; Eich, M.; Norwood, R. A. *Linear and Nonlinear Optics of Organic Materials III*; Proceedings of SPIE; SPIE: San Diego, CA, 2003; p 4. (f) Leclerc, N.; Sanaur, S.; Galmiche, L.; Mathevet, F.; Attias, A.-J.; Fave, J.-L.; Roussel, J.; Hapiot, P.; Lemaýtre, N.; Geffroy, B. *Chem. Mater*. **2005**, *17*, 502.

(5) (a) Thompson, M. E.; Djurovich, P. E.; Barlow, S.; Marder, S. R. *Comprehensive Organometallic Chemistry III*; O'Hare, D., Crabtree, R. H., Mingos, D. M. P., Eds.; Elsevier: Oxford, 2006; Vol. *12*. (b) Morall, J. P.; Dalton, G. T.; Humphrey, M. G.; Samoc, M. *Adv. Organomet. Chem*. **2008**, *55*, 61. (c) Coe, B. J. in Ref 1c; Chapter 18, p 571.

(6) Selected review articles and cited references: (a) Powell, C. E.; Humphrey, M. G. *Coord. Chem. Rev*. **2004**, *248*, 725. (b) Peris, E. *Coord. Chem. Rev*. **2004**, *248*, 279. (c) Barlow, S.; Marder, S. R. *Chem. Commun*. **2000**, 1555. (d) Heck, J.; Dabek, S.; Meyer-Friedrichsen, T.; Wong, H. *Coord. Chem. Rev*. **1999**, *190−192*, 1217. (e) Long, N. J. *Angew. Chem., Int. Ed. Engl*. **1995**, *34*, 21.

(7) (a) Di Bella, S.; Dragonetti, C.; Pizzotti, M.; Roberto, D.; Tessore, F.; Ugo, R. *Top. Organomet. Chem*. **2010**, *28*, 1. (b) Di Bella, S. *Chem. Soc. Rev*. **2001**, *30*, 355. (c) Coe, B. J.; Curati, N. R. M. *Comments Inorg. Chem*. **2004**, *25*, 147.

(8) Coe, B. J. In *Comprehensive Coordination Chemistry II*; McCleverty, J. A., Meyer, T. J., Eds.; Elsevier Pergamon: Oxford, 2004; Vol. *9*, pp 621.

(9) Selected review articles and cited references: (a) Le Bozec, H.; Renouard, T. *Eur. J. Inorg. Chem*. **2000**, 229. (b) Maury, O.; Le Bozec, H. *Acc. Chem. Res*. **2005**, *38*, 691. (c) Andraud, C.; Maury, O. *Eur. J. Inorg. Chem*. **2009**, 4357. (d) Calvete, M.; Yang, G. Y.; Hanack, M. *Synth. Met*. **2004**, *141*, 231. (e) Cariati, E.; Pizzotti, M.; Roberto, D.; Tessore, F.; Ugo, R. *Coord. Chem. Rev*. **2006**, *250*, 1210.

(10) (a) *The Chemistry of the Carbon-Nitrogen Double Bond*; Patai, S., Ed.; Wiley: New York, 1970. (b) Holm, R. H.; Everett, G. W.; Chakravorty, A. *Prog. Inorg. Chem*. **1966**, *7*, 183.

(11) (a) Lacroix, P. G. *Eur. J. Inorg. Chem*. **2001**, 339 and references cited therein. (b) Di Bella, S.; Fragala, I. *Synth. Met*. **2000**, *115*, 191 and references cited therein.

(12) (a) Averseng, F.; Lacroix, P. G.; Malfant, I.; Dahan, I.; Nakatani, K. *J. Mater. Chem*. **2000**, *10*, 1013. (b) Averseng, F.; Lacroix, P. G.; Malfant, I.; Périssé, N.; Lepetit, C.; Nakatani, K. *Inorg. Chem*. **2001**, *40*, 3797. (c) Lacroix, P. G.; Averseng, F.; Malfant, I.; Nakatani, K. *Inorg. Chim. Acta* **2004**, *357*, 3825. (d) Margeat, O.; Lacroix, P. G.; Costes, J.-P.; Donnadieu, B.; Lepetit, C.; Nakatani, K. *Inorg. Chem*. **2004**, *43*, 4743. (e) Costes, J.-P.; Lamère, J.-F.; Lepetit, C.; Lacroix, P. G.; Dahan, F.; Nakatani, K. *Inorg. Chem*. **2005**, *44*, 1973.

(13) (a) Di Bella, S.; Fragala, I.; Ledoux, I.; Zyss, J. *Chem.—Eur. J*. **2001**, *7*, 3738. (b) Di Bella, S.; Fragala, I. *New J. Chem*. **2002**, *26*, 285. (c) Di Bella, S.; Fragala, I.; Guerri, A.; Dapporto, P.; Nakatani, K. *Inorg. Chim. Acta* **2004**, *357*, 1161. (d) Di Bella, S.; Consiglio, G.; Leonardi, N.; Failla, S.; Finocchiaro, P.; Fragala, I. *Eur. J. Inorg. Chem*. **2004**, 2701.

(14) (a) Rigamonti, L.; Demartin, F.; Forni, A.; Righetto, S.; Pasini, A. *Inorg. Chem*. **2006**, *45*, 10976. (b) Gradinaru, J.; Forni, A.; Druta, V.; Tessore, F.; Zecchin, S.; Quici, S.; Garbalau, N. *Inorg. Chem*. **2007**, *46*, 884.

(15) For third-order NLO properties, see: (a) Floyd, J. M.; Gray, G. M.; VanEngen Spivey, A. G.; Lawson, C. M.; Pritchett, T. M.; Ferry, M. J.; Hoffman, R. C.; Mott, A. G. *Inorg. Chim. Acta* **2005**, *358*, 3773. (b) Tedim, J.; Patrício, S.; Bessada, R.; Morais, R.; Sousa, C.; Marques, M. B.; Freire, C. *Eur. J. Inorg. Chem*. **2006**, 3425.

(16) (a) Di Bella, S.; Fragala, I.; Ledoux, I.; Diaz-Garcia, M. A.; Marks, T. J. *J. Am. Chem. Soc*. **1997**, *119*, 9550. (b) Di Bella, S.; Fragala, I.; Ledoux, I.; Marks, T. J. *J. Am. Chem. Soc*. **1995**, *117*, 9481.

and redox switching abilities.[19] On the other hand, its cationic electron-withdrawing isolobal counterparts, namely, the robust mixed sandwich derivatives $[Cp'M(\eta^6\text{-arene})]^+$, (M = Fe, Ru; Cp′ = Cp = η^5-C_5H_5, Cp′ = Cp* = η^5-C_5Me_5),[20] have also proven their efficiency as an organometallic chromophore to achieve second order NLO responses.[21] On the basis of the considerations above, we developed an approach which utilizes the advantages of both ferrocenyl and $[Cp^*Ru(\eta^6\text{-arene})]^+$ units (ferrocenyl = $CpFe(\eta^5\text{-}C_5H_4)$), such as chemical and thermal stability, three-dimensional structure, and aromatic chemistry, for obtaining heterotrinuclear π−conjugated donor−acceptor unsymmetrical Schiff base complexes (Chart 1, type **B** with R = ferrocenyl and R′ = Cp^*Ru^+).[22] In such organometallic-inorganic hybrids, the ferrocenyl fragment was introduced as a preformed tridentate enaminone metalloligand,[23,24] while the cationic entity $[Cp^*Ru(\eta^6\text{-salicylidene})]^+$ was generated through a ligand exchange reaction with the arenophile source $[Cp^*Ru(NCCH_3)_3]PF_6$,[25] and both organometallic building blocks were linked together by a M^{II} classical Werner type coordination core {M(ONNO)} (M = Ni, Cu). The crucial role of this Cp^*Ru^+ moiety has very recently been highlighted by Sessler and co-workers in the chemistry of ruthenocene-porphyrin and ruthenocene-porphycene hybrid complexes, where they showed that the intrinsic electronic properties of the metalloporphyrins and metalloporphycenes are altered in a dramatic way upon fusion of the cationic arenophile to one or more pyrrolic subunits of these macrocycles.[26]

In branching such donor and acceptor organometallic end groups at the contour of the unsymmetrical Schiff base platform, one would expect some synergistic effects to occur, leading for instance to the enhancement of NLO properties of these new salen-type derivatives. Thus, to continue this work, two series of new D-π-A type compounds were designed and prepared, which consist of thermally stable organometallic substituted donor−acceptor nickel(II) and copper(II) unsymmetrical Schiff base complexes exhibiting second-order NLO responses, tunable by the metal center and the arenophile appendix, and a theoretical investigation allowing rationalization and substantiation of the experimental findings. The paper reports on the syntheses, spectroscopic characterization, electrochemical and linear optical properties of a family of binuclear M[Fc-C(O)CH=C(CH_3)N-X-N=CH-(2-O,5-R-C_6H_3)] (M = Ni (**4**), Cu (**5**), X = *o*-C_6H_4, R = H; M = Ni (**9**), X = CH_2CH_2, R = OH), and their corresponding ionic trinuclear inorganic NLO chromophores [M{Fc-C(O)CH=C-(CH_3)N-X-N=CH-(η^6-2-O,5-R-C_6H_3)RuCp^*}][PF_6] (**6**, **7**, **10**), as well as of the new metalloligand precursor [Fc-C(O)CH=C(CH_3)N(H)CH_2CH_2N=CH-(2,5-$(OH)_2C_6H_3$)] (**8**), and the X-ray structural determinations of **4** and **8**. We report also the values of the first hyperpolarizability (β) of selected compounds obtained from Harmonic Light Scattering (HLS) experiments. In addition, the optimized geometries of all compounds were obtained by density functional theory (DFT) computational studies. Moreover, DFT and its time-dependent DFT extension (TDDFT) provide a rationalization of the electrochemical and spectroscopic properties, and analyzes the electronic communication between the metal centers.

Experimental Section

Materials. All manipulations were carried out under a dinitrogen atmosphere using standard Schlenk techniques. The solvents were dried and distilled according to standard procedures. Ethylenediamine, *o*-phenylenediamine, 2-hydroxobenzaldehyde (salicylaldehyde), 2,5-dihydroxobenzaldehyde (5-hydroxosalicylaldehyde), nickel(II) acetate tetrahydrate, and copper(II) acetate monohydrate were purchased from Aldrich and used without further purification. The organometallic tridentate "half units" $CpFe(\eta^5\text{-}C_5H_4)$-C(O)CH=C-($CH_3$)N(H)-*o*-$C_6H_4NH_2$) (**1**),[23] and $CpFe(\eta^5\text{-}C_5H_4)$-C(O)CH=C($CH_3$)N(H)$C_2H_4NH_2$ (**2**),[22b] pentamethylcyclopentadienyltris(acetonitrile) ruthenium(II) hexafluorophosphate,[25,27] and pentamethylcyclopentadienyl(η^6-salicylaldehyde)ruthenium hexafluorophosphate[28] were synthesized using the established literature procedures. The synthesis and spectroscopic characterization of the heterobinuclear iron−ruthenium metalloligand **3** is provided in the Supporting Information.

Characterization and Instrumentation. Solid IR spectra were recorded on a Perkin-Elmer, Model Spectrum One, FT-IR spectrophotometer with KBr disks in the 4000 to 400 cm^{-1} range. Electronic spectra were obtained with a Spectronic, Genesys 2, spectrophotometer. The ^1H and ^{13}C NMR spectra were recorded on either Bruker Avance 400 Digital or Avance 500 Instruments. All NMR spectra are reported in parts per million (ppm, δ) relative to tetramethylsilane (Me_4Si), with the residual solvent proton resonance and carbon resonances used as internal standards. Coupling constants (*J*) are reported in

(17) (a) Rosenblum, M. *Chemistry of the Iron Group Metallocenes*; Wiley: New York, 1965. (b) Neuse, E. W.; Woodhouse, J. R.; Montaudo, G.; Puglis, C. *Appl. Organomet. Chem.* **1988**, *2*, 53. (c) *Ferrocenes: Homogenous Catalysis, Organic Synthesis, Materials Science*; Togni, A., Hayashi, Eds.; Wiley-VCH: Weinheim, 1995. (d) *Ferrocenes: Ligands, Materials and Biomolecules*; Stepnicka, P., Ed.; Wiley-VCH: Weinheim, 2008.

(18) (a) Kinnibrugh, T. L.; Salman, S.; Getmanenko, Y. A.; Coropceanu, V.; Porter, W. W.; Timofeeva, T. V.; Matzger, A. J.; Brédas, J.-L.; Marder, S. R.; Barlow, S. *Organometallics* **2009**, *28*, 1350, and references cited therein. (b) Kondo, M.; Uchikawa, M.; Namiki, K.; Zhang, W.-W.; Kume, S.; Nishibori, E.; Suwa, H.; Aoyagi, S.; Sakata, M.; Murata, M.; Kobayashi, Y.; Nishihara, H. *J. Am. Chem. Soc.* **2009**, *131*, 12112. (c) Liao, Y.; Eichinger, B. E.; Firestone, K. A.; Haller, M.; Luo, J. D.; Kaminsky, W.; Benedict, J. B.; Reid, P. J.; Jen, A. K. Y.; Dalton, L. R.; Robinson, B. H. *J. Am. Chem. Soc.* **2005**, *127*, 2758.

(19) (a) Malaun, M.; Reeves, Z. R.; Paul, R. L.; Jeffery, J. C.; McCleverty, J. A.; Ward, M. D.; Asselberghs, I.; Clays, K.; Persoons, A. *Chem. Commun.* **2001**, 49. (b) Asselberghs, I.; Clays, K.; Persoons, A.; McDonagh, A. M.; Ward, M. D.; McCleverty, J. A. *Chem. Phys. Lett.* **2003**, *368*, 408.

(20) Astruc, D. *Organometallic Chemistry and Catalysis*; Springer: Heidelberg, 2007; Chapter 11, p 241.

(21) (a) Fuentealba, M.; Toupet, L.; Manzur, C.; Carrillo, D.; Ledoux-Rak, I.; Hamon, J.-R. *J. Organomet. Chem.* **2007**, *692*, 1099. (b) Millán, L.; Fuentealba, M.; Manzur, C.; Carrillo, D.; Faux, N.; Caro, B.; Robin-Le Guen, F.; Sinbandhit, S.; Ledoux-Rak, I.; Hamon, J.-R. *Eur. J. Inorg. Chem.* **2006**, 1131. (c) Lambert, C.; Gaschler, W.; Zabel, M.; Matschiner, R.; Wortmann, R. *J. Organomet. Chem.* **1999**, *592*, 109.

(22) (a) Fuentealba, M.; Hamon, J.-R.; Carrillo, D.; Manzur, C. *New J. Chem.* **2007**, *31*, 1815. (b) Trujillo, A.; Sinbandhit, S.; Toupet, L.; Carrillo, D.; Manzur, C.; Hamon, J.-R. *J. Inorg. Organomet. Polym. Mater.* **2008**, *18*, 81.

(23) Fuentealba, M.; Trujillo, A.; Hamon, J.-R.; Carrillo, D.; Manzur, C. *J. Mol. Struct.* **2008**, *881*, 76.

(24) Hu, P.; Zhang, L.; Zhu, X.; Liu, X.; Ji, L.; Chen, Y. *Polyhedron* **1989**, *8*, 2459.

(25) Fagan, P. J.; Ward, M. D.; Calabrese, J. C. *J. Am. Chem. Soc.* **1989**, *111*, 1698.

(26) (a) Cuesta, L.; Karnas, E.; Lynch, V. M.; Sessler, J. L.; Kajonkijya, W.; Zhu, W.; Zhang, M.; Ou, Z.; Kadish, K. M.; Ohkubo, K.; Fukuzumi, S. *Chem.—Eur. J.* **2008**, *14*, 10206. (b) Cuesta, L.; Karnas, E.; Lynch, V. M.; Chen, P.; Shen, J.; Kadish, K. M.; Ohkubo, K.; Fukuzumi, S.; Sessler, J. L. *J. Am. Chem. Soc.* **2009**, *131*, 13538.

(27) Mbaye, M. D.; Demerseman, B.; Renaud, J.-L.; Toupet, L.; Bruneau, C. *Adv. Synth. Catal.* **2004**, *346*, 835.

(28) The procedure used to prepare the corresponding triflate salt was followed: Wheeler, D. E.; Baetz, N. W.; Holder, G. N.; Hill, S. T.; Milos, S.; Luczak, K. A. *Inorg. Chim. Acta* **2002**, *328*, 210.

Chart 2. Labeling Scheme Used for NMR Assignments

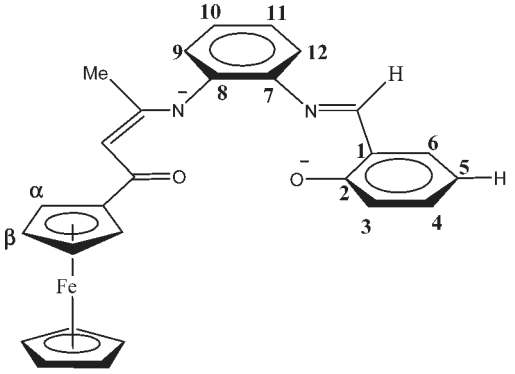

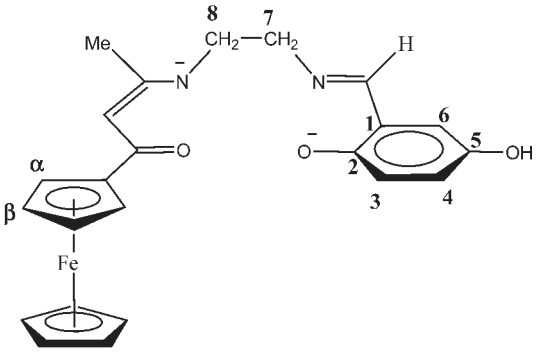

hertz (Hz), and integrations are reported as number of protons. The following abbreviations are used to describe peak patterns: s = singlet, d = doublet, t = triplet, m = multiplet, br = broad. ^{1}H and ^{13}C NMR chemical shift assignments are supported by data obtained from ^{1}H−^{1}H COSY, ^{1}H−^{13}C HMQC, and ^{1}H−^{13}C HMBC NMR experiments, and are given according to the numbering scheme of Chart 2. High resolution electrospray ionization mass spectra (ESI-MS) were obtained at the Centre Régional de Mesures Physiques de l'Ouest (CRMPO, Rennes) on a MS/MS ZabSpec TOF Micromass spectrometer (4 kV). Poly(ethylene glycol) (PEG) was used as internal reference and dichloromethane was used as solvent. Elemental analyses were conducted on a Thermo-FINNIGAN Flash EA 1112 CHNS/O analyzer by the Microanalytical Service of the CRMPO at the University of Rennes 1, France. Cyclic voltammetry (CV) measurements were performed using a Radiometer Analytical model PGZ 100 all-in one potentiostat, using a standard three-electrode setup with a vitreous carbon or a platinum disk working electrode, platinum wire auxiliary electrode, and Ag/AgCl as the reference electrode. Dichloromethane solutions were 1.0 mM in the compound under study and 0.1 M in the supporting electrolyte n-$Bu_4N^+PF_6^-$ with the voltage scan rate = 100 mV s^{-1}. Under these experimental conditions the ferrocene/ferrocenium couple, used as an internal reference for the potential measurements, was located at $E_{1/2}$ = 0.560 V (ΔE_p = 82 mV). $E_{1/2}$ is defined as equal to $(E_{pa} + E_{pc})/2$, where E_{pa} and E_{pc} are the anodic and cathodic peak potentials, respectively. Melting points were determined in evacuated capillaries and were not corrected.

Synthesis of Ni[CpFe(η^5-C_5H_4)-C(O)CH=C(CH_3)N-*o*-C_6H_4-N=CH-(2−O-C_6H_4)] (4). To a Schlenk tube containing a stirred solution of CpFe(η^5-C_5H_4)-C(O)CH=C(CH_3)N(H)-*o*-$C_6H_4NH_2$ (**1**) (400 mg, 1.11 mmol) in ethanol (30 mL) was added dropwise 120 μL of salicylaldehyde (1.11 mmol). The resulting solution was stirred for 15 min at room temperature (RT). A solution of nickel acetate tetrahydrate (553 mg, 2.22 mmol) in ethanol (10 mL) was then added, and the resulting solution was refluxed for 4 h. The mixture was allowed to cool to RT overnight. Evaporation of the solution to half of its volume under vacuum gave a purple microcrystalline precipitate. The solid material was filtered off, washed with methanol (2 × 3 mL), and dried in vacuo. Yield 151 mg, 26%. Slow evaporation of a concentrated dichloromethane solution deposited X-ray quality crystals. Mp 218 °C (dec). Anal. Calcd for $C_{27}H_{22}FeN_2NiO_2$: C, 62.24; H, 4.26; N, 5.38. Found: C, 62.14; H, 4.34; N, 5.24. IR (KBr, cm^{-1}): 3047(w) ν(C−H arom); 2963(w), 2920(w), 2852(w) ν(C−H aliph); 1606−1519(m) ν(C···O), ν(C···C) and/or ν(C···N); 1279(vw) ν(C−O). ^{1}H NMR (500 MHz, $CDCl_3$): δ 2.42 (s, 3H, CH_3), 4.20 (s, 5H, Cp), 4.36 (br t, $^3J_{HH}$ = 1.7 Hz, 2H, H$_\beta$ C_5H_4), 4.77 (br t, $^3J_{HH}$ = 1.7 Hz, 2H, H$_\alpha$ C_5H_4), 5.64 (s, 1H, CH=C), 6.61 (t, $^3J_{HH}$ = 7.4 Hz, 1H, H-5), 6.96 (t, $^3J_{HH}$ = 7.8 Hz, 1H, H-11), 7.06 (m, 2H, H-3 and H-10), 7.25 (t, $^3J_{HH}$ = 7.4 Hz, 1H, H-4), 7.26 (d, $^3J_{HH}$ = 7.8 Hz, 1H, H-9), 7.32 (br d, $^3J_{HH}$ = 7.4 Hz, 1H, H-6), 7.60 (d, $^3J_{HH}$ = 7.8 Hz, 1H, H-12), 8.15 (s, 1H, N=CH). ^{13}C{^{1}H} NMR (125 MHz, $CDCl_3$): δ 24.68 (CH_3), 68.73 (C_α C_5H_4), 70.07 (Cp), 70.62 (C_β C_5H_4), 79.79 (C_{ipso} C_5H_4), 102.81 (*C*H=C), 114.37 (C-12), 115.46 (C-5), 120.21 (C-1), 121.64 (C-9), 121.97 (C-3), 122.78 (C-11), 126.20 (C-10), 132.99 (C-6), 134.47 (C-4), 142.42 (C-7), 145.32 (C-8), 162.23 (CH=*C*), 165.56 (C-2), 180.18 (C=O).

Synthesis of Cu[CpFe(η^5-C_5H_4)-C(O)CH=C(CH_3)N-*o*-C_6H_4-N=CH-(2−O-C_6H_4)] (5). The synthesis of this orange complex was carried out following a procedure similar to that described above for complex **4**, using in this case 400 mg (1.10 mmol) of **1**, 117 μL (1.10 mmol) of salicylaldehyde and 215 mg (1.10 mmol) of copper acetate monohydrate. Yield 256 mg, 44%. Mp 213 °C (dec). Anal. Calcd for $C_{27}H_{22}CuFeN_2O_2 \cdot 0.5CH_2Cl_2$ (crystallization solvent): C, 58.12; H, 4.08; N, 4.93. Found: C, 58.47; H, 4.22; N, 4.87. ESI MS (*m*/*z*), calcd for $C_{27}H_{22}N_2O_2{}^{56}Fe^{63}Cu$: 525.03267, found: 525.0326 [M]. IR (KBr, cm^{-1}): 3089(w) ν(C−H arom); 2991(w), 2922(w), 2859(w) ν(C−H aliph); 1615−1520(m) ν(C···O), ν(C···C) and/or ν(C···N); 1278(vw) ν(C−O).

Synthesis of [Ni{CpFe(η^5-C_5H_4)-C(O)CH=C(CH_3)N-*o*-C_6H_4-N=CH-(η^6-2−O-C_6H_4)RuCp*}][PF_6] (6). A Schlenk tube was charged with complex **3** (150 mg, 0.20 mmol), nickel acetate tetrahydrate (45 mg, 0.2 mmol), methanol (10 mL), and a magnetic stir bar. The reaction mixture was stirred for 2 h at RT while a dark precipitate formed. The solid material was filtered, washed with diethyl ether (2 × 5 mL), and recrystallized from CH_2Cl_2/Et_2O mixture as a brown-violet crystalline solid. Yield 121 mg, 66%. Mp 203 °C. Anal. Calcd for $C_{37}H_{37}F_6FeN_2O_2NiPRu$: C, 49.25; H, 4.13; N, 3.11. Found: C, 48.87; H, 3.93; N, 3.05. ESI MS (*m*/*z*), calcd for $C_{37}H_{37}N_2O_2{}^{56}Fe^{58}Ni^{102}Ru$: 757.06014, found: 757.0606 [M-(PF_6)]. IR (KBr, cm^{-1}): 3047(w) ν(C−H arom); 2963(w), 2920(w), 2852(w) ν(C−H aliph); 1606−1519(m) ν(C···O), ν(C···C) and/or ν(C···N); 1286(w) ν(C−O); 840(s) ν(PF_6); 557(s) δ(P−F). ^{1}H NMR (500 MHz, acetone-d_6): δ 2.10 (s, 15H, $C_5(CH_3)_5$), 2.50 (s, 3H, CH_3), 4.24 (s, 5H, Cp), 4.47 (m, 1H, H$_\beta$ C_5H_4), 4.48 (m, 1H, H$_{\beta'}$ C_5H_4), 4.78 (m, 1H, H$_\alpha$ C_5H_4), 4.80 (m, 1H, H$_{\alpha'}$ C_5H_4), 5.76 (d, $^3J_{HH}$ = 6.4 Hz, 1H, H-3), 5.87 (s, 1H, CH=C), 5.86 (t, $^3J_{HH}$ = 5.8 Hz, 1H, H-5), 5.94 (t, $^3J_{HH}$ = 5.8 Hz, 1H, H-4), 6.35 (d, $^3J_{HH}$ = 5.3 Hz, 1H, H-6), 7.07 (t, $^3J_{HH}$ = 7.5 Hz, 1H, H-11), 7.31 (t, $^3J_{HH}$ = 7.5 Hz, 1H, H-10), 7.50 (d, $^3J_{HH}$ = 7.5 Hz, 1H, H-9), 7.98 (d, $^3J_{HH}$ = 7.5 Hz, 1H, H-12), 8.83 (s, 1H, N=CH). ^{13}C{^{1}H} NMR (125 MHz, acetone-d_6): δ 10.56 ($C_5(CH_3)_5$), 24.59 (CH_3), 69.27 (C_α C_5H_4), 69.64 ($C_{\alpha'}$ C_5H_4), 70.87 (Cp), 71.87 (C_β C_5H_4), 71.91 ($C_{\beta'}$ C_5H_4), 79.64 (C-3), 79.65 (C_{ipso} C_5H_4), 82.06 (C-1), 84.93 (C-5), 89.13 (C-6), 89.63 (C-4), 95.56 ($C_5(CH_3)_5$), 104.00 (*C*H=C), 116.75 (C-12), 123.06 (C-9), 124.39 (C-11), 130.25 (C-10), 139.69 (C-2), 142.14 (C-7), 146.96 (C-8), 160.44 (N=CH), 164.38 (CH=*C*), 181.40 (C=O).

Synthesis of [Cu{CpFe(η^5-C_5H_4)-C(O)CH=C(CH_3)N-*o*-C_6H_4-N=CH-(η^6-2−O-C_6H_4)RuCp*}][PF_6] (7). The synthesis of this dark orange complex was carried out following a procedure similar to that described above for complex **6**, using in this case, 200 mg (0.24 mmol) of **3** and 53.4 mg (0.24 mmol) of copper acetate

monohydrate. Yield 124 mg, 57%. Mp 281 °C. Anal. Calcd for $C_{37}H_{37}CuF_6FeN_2O_2PRu$: C, 48.98; H, 4.11; N, 3.08. Found: C, 48.72; H, 3.92; N, 2.85 ESI MS (*m*/*z*), calcd for $C_{37}H_{37}N_2O_2{}^{56}Fe^{63}Cu^{102}Ru$: 762.05439, found: 762.0558 [M-(PF_6)]. IR (KBr, cm^{-1}): 3093(w) ν(C−H arom); 2964(w), 2918(w), 2854(w) ν(C−H aliph); 1616−1519(m) ν(C···O), ν(C···C) and/or ν(C···N); 1285(w) ν(C−O); 841(s) $\nu(PF_6)$; 557(m) δ(P−F).

Synthesis of CpFe(η^5-C_5H_4)-C(O)CH=C(CH_3)N(H)CH_2-CH_2N=CH-(2,5-$(OH)_2$-C_6H_3) (8). A round-bottom 50 mL flask equipped with a reflux condenser was loaded with CpFe(η^5-C_5H_4)-C(O)CH=C(CH_3)N(H)$CH_2CH_2NH_2$ (**2**) (300 mg, 0.98 mmol), 2,5-dihydroxobenzaldehyde (133.6 mg, 0.98 mmol), a magnetic stir bar, and dichloromethane (10 mL). The reaction mixture was stirred and refluxed for 2 h while a red precipitate formed. At RT, it was filtered off and washed with CH_2Cl_2 (3 × 5 mL) and dried under vacuum. X-ray quality crystals were obtained by recrystallization from hot dichloromethane. Yield 310 mg, 72%. Mp 204−206 °C. Anal. Calcd for $C_{23}H_{24}FeN_2O_3$: C, 63.90; H, 5.59; N, 6.48. Found: C, 63.77; H, 5.57; N, 6.54. ESI MS (*m*/*z*), calcd for $C_{23}H_{24}N_2O_3Na^{56}Fe$: 455.10340, found: 455.1055 [M+Na]. IR (KBr, cm^{-1}): 3109(w) ν(O−H); 3088(w), 3053(vw) ν(C−H arom); 2996(vw), 2954(vw), 2907(vw) ν(C−H aliph); 1639(w), 1595(m), 1535(m) ν(C···O), ν(C···C) and/or ν(C···N), 1305(w) δ(OH). ^{1}HNMR (400 MHz, DMSO-d_6): δ 1.95 (s, 3H, CH_3), 3.02 (q, $^3J_{HH}$ = 5.4 Hz, 2H, H-8), 3.75 (t, $^3J_{HH}$ = 5.8 Hz, 2H, H-7), 4.08 (s, 5H, Cp), 4.29 (t, $^3J_{HH}$ = 1.9 Hz, 2H, H$_\beta$ C_5H_4), 4.65 (t, $^3J_{HH}$ = 1.9 Hz, 2H, H$_\alpha$ C_5H_4), 5.32 (s, 1H, CH=C), 6.51 (d, $^3J_{HH}$ = 8.8 Hz, 1H, H-3), 6.76 (d, $^3J_{HH}$ = 2.9 Hz, 1H, H-6), 6.72 (dd, $^3J_{HH}$ = 8.8 Hz, $^4J_{HH}$ = 2.4 Hz, 1H, H-4), 8.48 (t, $^3J_{HH}$ = 5.8 Hz, 1H, N=CH), 8.98 (s, 1H, OH), 10.86 (t, $^3J_{HH}$ = 5.8 Hz, 1H, NH), 12.34 (s, 1H, OH). $^{13}C\{^1H\}$ NMR (100 MHz, DMSO-d_6): δ 18.93 (CH_3), 43.14 (C-8), 59.01 (C-7), 67.94 (C_α C_5H_4), 69.30 (Cp) 70.06 (C_β C_5H_4), 82.95 (C_{ipso} C_5H_4), 92.60 (*C*H=C), 116.48 (C-6), 116.84 (C-1), 118.55 (C-3), 119.93 (C-4), 149.31 (C-5), 152.88 (C-2), 162.14 (N=CH), 166.94 (CH=*C*), 190.09 (C=O).

Synthesis of Ni[CpFe(η^5-C_5H_4)-C(O)CH=C(CH_3)NCH_2-CH_2N=CH-(2-O,5-OH-C_6H_3)] (9). A solution of 2,5-dihydroxobenzaldehyde (220.7 mg, 1.59 mmol) in CH_2Cl_2 (3 mL) and methanol (5 mL) was added dropwise to a stirred solution of compound **2** (500 mg, 1.60 mmol) in CH_2Cl_2 (3 mL). The resulting solution was stirred for 10 min at RT. A solution of nickel acetate tetrahydrate (455.7 mg, 1.60 mmol) in methanol (3 mL) was then added by cannula, and the resulting solution was heated at reflux for 2 h. Upon cooling to RT, a brown orange precipitate formed. The solid was collected by filtration, washed with CH_2Cl_2 (2 × 5 mL), and dried under vacuum. Yield 553 mg, 71%. Mp 279 °C (dec). Anal. Calcd for $C_{23}H_{22}FeN_2NiO_3 \cdot CH_2Cl_2$ (crystallization solvent): C, 50.35; H, 4.20; N, 4.90. Found: C, 50.16; H, 4.38; N, 4.88. ESI MS (*m*/*z*), calcd for $C_{23}H_{22}N_2O_3{}^{56}Fe^{58}Ni$: 488.03333, found: 488.0328 [M]. IR (KBr, cm^{-1}): 3128(w) ν(O−H); 3085(w), 3069(w) ν(C−H arom); 2941(w), 2923(w), 2844(w) ν(C−H aliph); 1619(m), 1575(m), 1544(m) ν(C···O), ν(C···C) and/or ν(C···N); 1297(m) δ(OH). ^{1}H NMR (500 MHz, DMSO-d_6): δ 1.97 (s, 3H, CH_3), 3.02 (t, $^3J_{HH}$ = 6.8 Hz, 2H, H-8), 3.37 (t, $^3J_{HH}$ = 6.8 Hz, 2H, H-7), 4.14 (s, 5H, Cp), 4.29 (t, $^3J_{HH}$ = 1.9 Hz, 2H, H$_\beta$ C_5H_4), 4.56 (t, $^3J_{HH}$ = 1.9 Hz, 2H, H$_\alpha$ C_5H_4), 5.42 (s, 1H, CH=C), 5.80 (s, 2H, CH_2Cl_2), 6.51 (d, $^3J_{HH}$ = 9.0 Hz, 1H, H-3), 6.57 (d, $^3J_{HH}$ = 3.2 Hz, 1H, H-6), 6.72 (dd, $^3J_{HH}$ = 9.0 Hz, $^4J_{HH}$ = 3.2 Hz, 1H, H-4), 7.68 (s, 1H, N=CH), 8.49 (s, 1H, OH). $^{13}C\{^1H\}$ NMR (125 MHz, DMSO-d_6): δ 21.32 (CH_3), 51.06 (C-8), 54.82 (CH_2Cl_2), 59.47 (C-7), 67.48 (C_α C_5H_4), 69.26 (C_β C_5H_4), 69.46 (Cp), 81.21 (C_{ipso} C_5H_4), 96.59 (*C*H=C), 114.49 (C-6), 119.21 (C-1), 120.19 (C-3), 123.67 (C-4), 145.43 (C-5), 158.24 (C-2), 161.27 (N=CH), 164.27 (CH=*C*), 173.91 (C=O).

Synthesis of [Ni{CpFe(η^5-C_5H_4)-C(O)CH=C(CH_3)NCH_2-CH_2N=CH-(η^6-2-O,5-OH-C_6H_3)RuCp*}][PF_6] (10). A Schlenk tube was loaded with [Cp*Ru($NCCH_3$)$_3$]PF_6 (175 mg, 0.35 mmol), compound **9** (170 mg, 0.35 mmol), a magnetic stir bar and CH_2Cl_2 (5 mL). The reaction mixture was stirred at RT overnight. The solvent was then evaporated under reduced pressure and the residue washed with diethyl ether (2 × 5 mL). The resulting solid was redissolved in CH_2Cl_2 (5 mL). The solution was filtered off and reduced to half of its volume. Addition of diethyl ether (10 mL) caused the formation of a red microcrystalline precipitate which was collected by filtration and dried under vacuum. Yield 133 mg, 44%. Mp 312 °C. Anal. Calcd for $C_{33}H_{37}F_6FeN_2NiO_3PRu$: C, 45.55; H, 4.28; N, 3.21. Found: C, 45.28; H, 4.06; N, 2.95. ESI MS (*m*/*z*), calcd for $C_{33}H_{37}N_2O_3{}^{56}Fe^{58}Ni^{102}Ru$: 725.05505, found: 725.0545 [M-(PF_6)]. IR (KBr, cm^{-1}): 3241(w) ν(O−H); 3088(w) ν(C−H arom); 2960(w), 2861(w) ν(C−H aliph); 1636(m), 1573(m), 1510(s) ν(C···O), ν(C···C) and/or ν(C···N); 1258(w) ν(C−O); 843(s) $\nu(PF_6)$; 558(s) δ(P−F). ^{1}H NMR (500 MHz, acetone-d_6): δ 2.05 (s, 3H, CH_3), 2.09 (s, 15H, $C_5(CH_3)_5$), 3.19 (m, 1H, H-8), 3.24 (m, 1H, H-8′), 3.57 (m, 1H, H-7), 3.61 (m, 1H, H-7′), 4.16 (s, 5H, Cp), 4.30 (br s, 1H, H$_\beta$ C_5H_4), 4.32 (br s, 1H, H$_{\beta'}$ C_5H_4), 4.63 (br s, 1H, H$_\alpha$ C_5H_4), 4.67 (br s, 1H, H$_{\alpha'}$ C_5H_4), 5.25 (s, 1H, CH=C), 5.48 (d, $^3J_{HH}$ = 6.3 Hz, 1H, H-3), 5.66 (br d, $^3J_{HH}$ = 6.3 Hz, 1H, H-4), 5.77 (br s, 1H, H-6), 7.96 (s, 1H, N=CH), 9.14 (br s, 1H, OH). $^{13}C\{^1H\}$ NMR (125 MHz, acetone-d_6): δ 10.22 ($C_5(CH_3)_5$), 21.59 (CH_3), 52.30 (C-8), 62.26 (C-7), 68.02 (C_α C_5H_4), 69.19 ($C_{\alpha'}$ C_5H_4), 70.52 (Cp), 70.56 (C_β C_5H_4), 70.60 ($C_{\beta'}$ C_5H_4), 76.19 (C-6), 77.42 (C-3), 79.06 (C-1), 79.31 (C-4), 81.48 C_{ipso} C_5H_4), 94.85 ($C_5(CH_3)_5$), 97.75 (*C*H=C), 126.64 (C-5), 138.14 (C-2), 165.97 (CH=*C*), 166.58 (N=CH), 175.77 (C=O).

Table 1. Crystal Data, Data Collection, and Structure Refinement Parameters for **4** and **8**

	4	**8**
empirical formula	$C_{27}H_{22}FeN_2NiO_2$	$C_{23}H_{24}FeN_2O_3$
formula mass, g mol^{-1}	521.03	432.29
collection *T*, K	298(2)	150(2)
crystal system	monoclinic	monoclinic
space group	$P2_1/c$	$P2_1/n$
a (Å)	9.9892(13)	12.1725(7)
b (Å)	18.584(3)	11.4739(6)
c (Å)	12.0417(16)	14.6825(8)
β (deg)	95.004(2)	97.7380(10)
V (Å^3)	2227.0(5)	2031.97(19)
Z	4	4
D_{calcd} (g cm^{-3})	1.554	1.413
crystal size (mm)	0.32 × 0.24 × 0.06	0.49 × 0.22 × 0.04
F(000)	1072	904
abs coeff (mm^{-1})	1.525	0.769
θ range (deg)	2.02 to 28.12	2.04 to 27.82
range *h*, *k*, *l*	−13/12, −24/23, −15/15	−15/15, −14/13, −18/19
no. total refl.	18572	15787
no. unique refl.	5032	4480
data/restraints/parameters	5032/0/299	4480/0/275
final *R* [$I > 2\sigma(I)$]	R_1 = 0.0544, wR_2 = 0.1074	R_1 = 0.0433, wR_2 = 0.0918
R indices (all data)	R_1 = 0.1018, wR_2 = 0.1234	R_1 = 0.0607, wR_2 = 0.1006
goodness of fit/F^2	0.993	1.038
largest diff. peak and hole (e Å^{-3})	0.578 and −0.324	0.435 and −0.249

X-ray Crystal Structure Determinations. Suitable X-ray single crystals of compounds **4** and **8** were obtained as described above and were mounted on top of glass fibers in a random orientation. Crystal data, data collection, and refinement parameters are given in Table 1. Compound **4** was studied at 298(2) K whereas complex **8** was studied at 150(2) K on a Bruker Smart Apex diffractometer equipped with bidimensional CCD detector employing graphite-monochromated Mo K_α radiation (λ = 0.71073 Å). Semiempirical corrections, via T-scans, were applied for absorption. The diffraction frames were integrated

using the SAINT package,[29] and corrected for absorption with SADABS.[30] The structures were solved using XS in SHELXTL-PC,[31] by direct methods and completed (non-H atoms) by difference Fourier techniques. The complete structure was then refined by the full-matrix least-squares procedures on reflection intensities (F^2).[32] The non-hydrogen atoms were refined with anisotropic displacement coefficients, and all hydrogen atoms were placed in idealized locations. CCDC reference numbers of compounds **4** and **8** are 646871 and 713025, respectively. These data can be obtained free of charge from the Cambridge Crystallographic Data Centre via www.ccdc.cam.ac.uk.

HLS Measurements. Because of the presence of ionic species in the series of compounds investigated here, we chose the HLS at 1.91 μm to measure the first order hyperpolarizabilities β of the molecules. The 1.91 μm fundamental beam was emitted by a high-pressure (30 bar), 50 cm long Raman cell pumped by a Nd^{3+}:YAG laser operating at 1.06 μm and providing pulses of 15 ns duration at a 10 Hz repetition rate. The backscattered 1.91 μm Raman emission was collected at a 45° incidence angle by use of a dichroic mirror, to eliminate most of the residual 1.06 μm pump photons. Choosing the 1.91 μm wavelength, whose harmonics at 955 nm is far from any resonance of the molecules to be investigated, prevents the contribution of possible two-photon fluorescence emission to the HLS signal. We have evidenced the absence of any wide-band two-photon fluorescence by checking that no HLS signal can be detected for wavelengths different from 955 nm. Our reference sample was a concentrated (10^{-2} M) solution of ethyl violet, its octupolar β value being 170×10^{-30} esu at 1.91 μm.[33] Chloroform (for neutral species) and dimethylformamide (DMF) (for the ionic compounds) solvents were used for the HLS measurements. Both solvents appear to be transparent at 1.91 μm. The HLS photons at 955 nm were focused onto a Hamamatsu R632−01 photomultiplier tube using two collecting lenses. The signal detected was then sampled and averaged using a boxcar, and processed by a computer. The reference beam was collected at a 45° incidence angle by a glass plate, and focused onto a highly nonlinear *N*-4-nitrophenyl-prolinol (NPP) powder, which was used as the frequency doubler. The variation of the scattered second harmonic intensity from the solution was recorded on the computer as a function of the reference second harmonic signal provided by the NPP powder, both signals scaling as the square of the incoming fundamental intensity. Values for β were then inferred from the slopes of the resulting lines.[34]

Computational Details. DFT[35] calculations were carried out using the Amsterdam Density Functional (ADF) program.[36] The Vosko−Wilk−Nusair parametrization[37] was used to treat electron correlation within the local density approximation, with gradient corrections added for exchange (Becke88)[38] and correlation (Perdew),[39] respectively. The numerical integration procedure applied for the calculation was developed by te Velde.[35d] The standard ADF TZP basis set was used for all the atoms. The frozen core approximation was used to treat core electrons at the following levels: Ru, 4p; Cu, 3p; Ni, 3p; Fe, 3p; C, 1s; N, 1s and O, 1s.[35d] Full geometry optimizations were carried out on each complex using the analytical gradient method implemented by Versluis and Ziegler.[40] The geometry for all the model compounds discussed in the text were fully optimized, with a good agreement between the computed geometric parameters and the available structural data. Spin-unrestricted calculations were carried out on all the odd-electrons and open-shell systems. The UV−visible electronic absorption transitions were computed on the DFT-optimized geometries using the TDDFT[41] method implemented within the ADF program, using the LB94 functional.

Results and Discussion

Synthesis and Common Spectral Characteristics. The investigated Schiff-base complexes were synthesized either by complexation of the organometallic ligands with the appropriate metal(II) ion or by one-pot template synthesis. In both cases, the reaction involves a condensation of the appropriate salicylaldehyde with the free amino group of the corresponding tridentate metalloligand. Thus, the neutral unsymmetrical Schiff base complexes **4** and **5** were readily synthesized by a well-known template procedure starting from the half-unit **1** bearing the *o*-phenylene amine arm,[23] an equimolar amount of salicylaldehyde, and nickel(II) acetate tetrahydrate and copper(II) acetate monohydrate, respectively, as outlined in Scheme 1. Heating this reaction mixture for 4 h in refluxing ethanol afforded compounds **4** and **5** that were isolated as violet and orange microcrystalline solids in 26 and 44% yield, respectively.

The corresponding ionic trinuclear counterparts usually result from the π-complexation of the salicylidene ring by the Cp^*Ru^+ arenophile (see below and Scheme 3). However, in the present cases, competitive complexation of both the central and terminal *o*-phenylenes forming the Schiff base skeleton of **4** and **5** might occur and give rise to untractable mixtures of compounds.[22b] Therefore, an alternative regioselective route to the unsymmetrical trinuclear Schiff base complex **6** and **7**, avoiding this competitive π-coordination, was designed. The first step consists in the preparation of the binuclear iron−ruthenium intermediate **3**, which is then treated with the appropriate metal acetate salt (Scheme 2). Thus, the organometallic salicylaldehyde brick $[Cp^*Ru(\eta^6\text{-}2\text{-}OH\text{-}C_6H_4CHO)][PF_6]$ was reacted with the metalloligand **1** in dichloromethane to provide, after stirring for 4 h at RT, an orange solid material that was isolated in 36% yield and identified as the expected heterobimetallic ligand **3** (see Supporting Information). The target organometallic-inorganic hybrids **6** and **7** were obtained by treatment of a

(29) *SAINT-PLUS*, Version 6.02; Bruker Analytical X-Ray Systems Inc.: Madison, WI, 1999.
(30) Sheldrick, G. M. *SADABS*, Version 2.05; Bruker Analytical X-Ray Systems Inc.: Madison, WI, 1999.
(31) *SHELXTL Reference Manual*, Version 6.14; Bruker Analytical X-Ray Systems Inc.: Madison, WI, 1998.
(32) Sheldrick, G. M. *SHELX97, Program for the Refinement of Crystal Structures*; University of Göttingen: Göttingen, Germany, 1997.
(33) Le Bozec, H.; Le Bouder, T.; Maury, O.; Bondon, A.; Ledoux, I.; Deveau, S.; Zyss, J. *Adv. Mater.* **2001**, *13*, 1677.
(34) Zyss, J.; ChauVan, T.; Dhenaut, C.; Ledoux, I. *Chem. Phys.* **1993**, *177*, 281.
(35) (a) Baerends, E. J.; Ellis, D. E.; Ros, P. *Chem. Phys.* **1973**, *2*, 41. (b) Baerends, E. J.; Ross, P. *Int. J. Quantum Chem.* **1978**, *S12*, 169. (c) Boerrigter, P. M.; te Velde, G.; Baerends, E. J. *Int. J. Quantum Chem.* **1988**, *33*, 87. (d) te Velde, G.; Baerends, E. J. J. *Comput. Phys.* **1992**, *99*, 84.
(36) *Amsterdam Density Functional* (*ADF*) *program*; Vrije Universiteit: Amsterdam, The Netherlands, 2005.
(37) Vosko, S. D.; Wilk, L.; Nusair, M. *Can. J. Chem.* **1990**, *58*, 1200.
(38) (a) Becke, A. D. *J. Chem. Phys.* **1986**, *84*, 4524. (b) Becke, A. D. *Phys. Rev. A* **1988**, *38*, 2098.
(39) (a) Perdew, J. P. *Phys. Rev. B* **1986**, *33*, 8882. (b) Perdew, J. P. *Phys. Rev. A* **1986**, *34*, 7406.
(40) Versluis, L.; Ziegler, T. *J. Chem. Phys.* **1988**, *88*, 322.
(41) (a) Casida, M. Time Dependent Functional Response Theory for Molecules. In *Recent Advances in Density Functional Methods*; Chong, D. P., Ed.; World Scientific: Singapore, 1995; Vol. *1*, p 155. (b) Gross, E. U. K.; Dobson, J. F.; Petersilka, M. In *Density Functional Theory*; Nalewajski, R. F., Ed.; Springer Series, Topics in Current Chemistry; Springer: Heidelberg, 1996. (c) van Gisbergen, S. J. A.; Snijders, J. G.; Baerends, E. J. *Comput. Phys.* **1999**, *118*, 119.
(42) Averseng, F.; Lacroix, P. G.; Malfant, I.; Lenoble, G.; Cassoux, P.; Nakatani, K.; Maltey-Fanton, I.; Delaire, J. A.; Aukauloo, A. *Chem. Mater.* **1999**, *11*, 995.

Scheme 1. Synthesis of the Neutral Binuclear Unsymmetrical Binuclear Schiff Base Complexes **4** and **5**

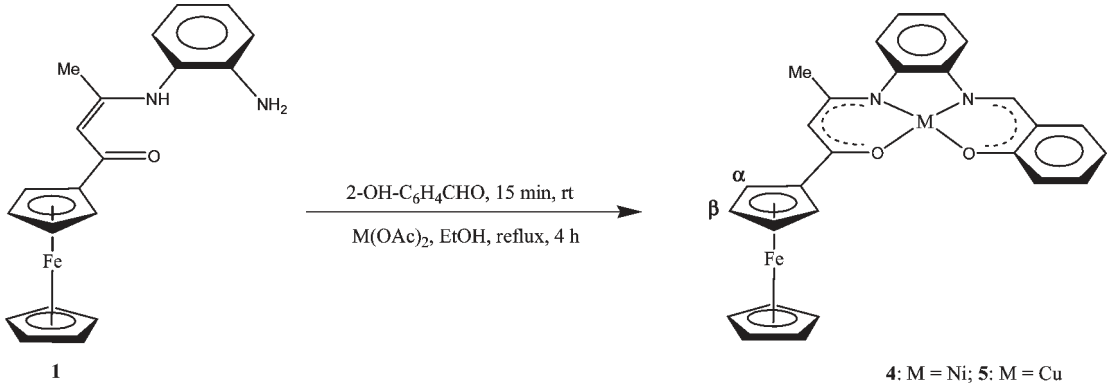

1 **4**: M = Ni; **5**: M = Cu

Scheme 2. Synthesis of the Ionic Unsymmetrical Trinuclear Schiff Base Complexes **6** and **7**

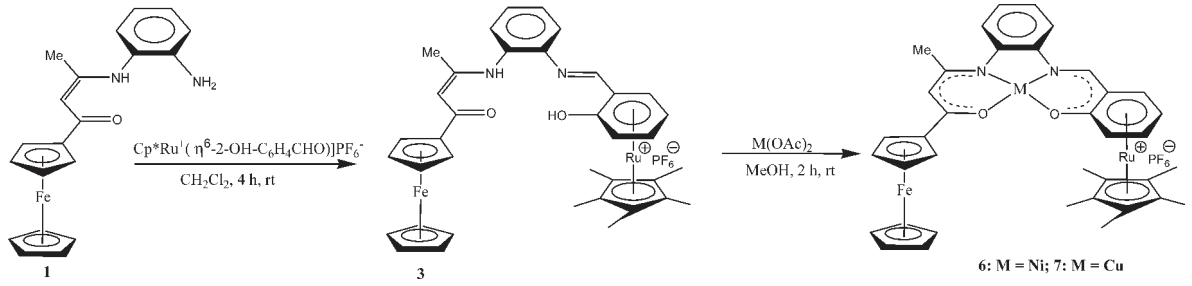

1 **3** **6**: M = Ni; **7**: M = Cu

Scheme 3. Synthesis of the 5-Functionalized Metalloligand **8** and of Its Bi- and Trinuclear Unsymmetrical Schiff Base Complexes **9** and **10**

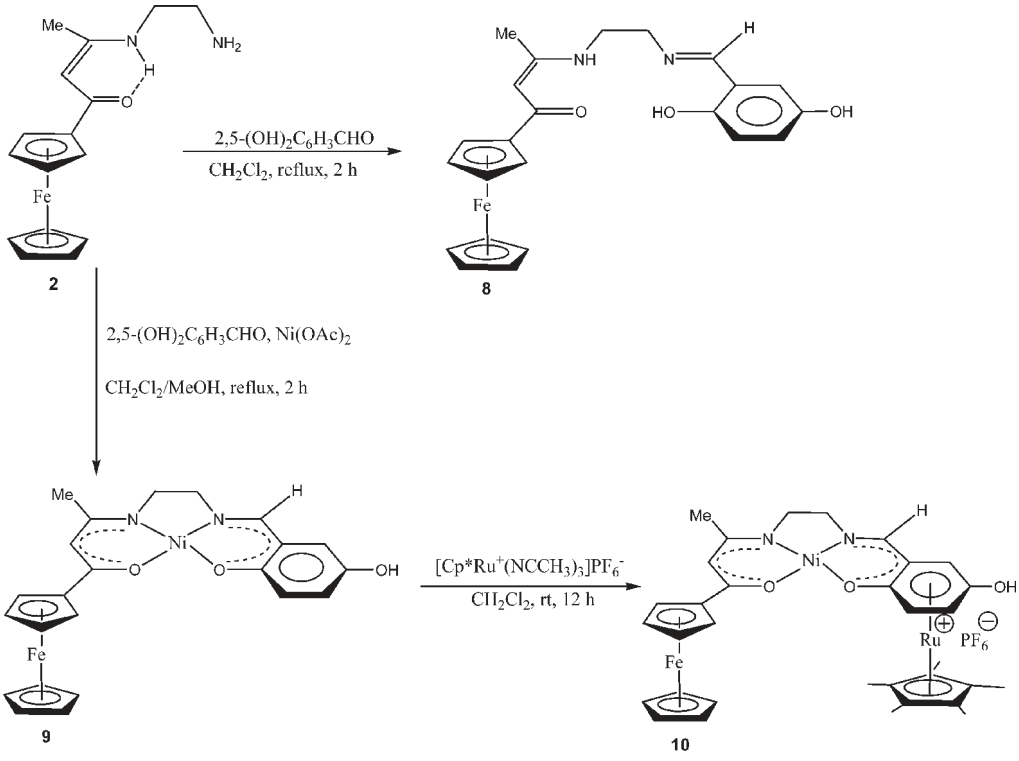

2 **8** **9** **10**

suspension of **3** in methanol with nickel(II) and copper(II) acetate salt, respectively (Scheme 2). The two products precipitated directly from the reaction mixture and were collected by filtration as brown-violet and dark orange solid materials in 66 and 57% yield, respectively.

The mono- (**8**), bi- (**9**) and trinuclear (**10**) salen-type complexes (Scheme 3) were targeted as scaffolds for the construction of donor−acceptor materials because of their simple structures with a potential single point of attachment, taking advantage of an efficient, straightforward, and inexpensive method for the synthesis of Schiff base ligands and their subsequent transition metal complexes.

Thus, the synthesis of the mononuclear functionalized Schiff base complex **8** was successfully accomplished by

direct condensation of the metalloligand **2** bearing the ethylene amine arm with 2,5-dihydroxobenzaldehyde for 2 h in refluxing dichloromethane (Scheme 3). The product precipitated directly from the reaction mixture and was isolated as a red powder in 72% yield. The corresponding neutral binuclear Schiff base complex **9** was prepared according to the template one-pot two-step procedure depicted above for **4** and **5**. The metalloligand **2** was reacted with 2,5-dihydroxobenzaldehyde and then with hydrated nickel(II) acetate in refluxing CH_2Cl_2/MeOH (1:1) mixture for 2 h. Compound **9** was isolated as a brown-orange powder in 71% yield. Treating this binuclear Schiff base precursor **9** with 1 equiv of the arenophile source $[Cp^*Ru(NCCH_3)_3][PF_6]$ overnight in dichloromethane at RT gave a clean conversion to the corresponding ionic trinuclear counterpart **10**, isolated as a red microcrystalline solid in 44% yield (Scheme 3). Note that **10** as well as the two other trinuclear complexes **6** and **7** contain the neutral electron-releasing ferrocenyl subunit and the cationic electron-withdrawing mixed sandwich, $[Cp^*Ru(\eta^6$-salicylidene$)]^+$, linked by a M^{II} classical Werner type coordination sets [M(ONNO)] (M = Ni, Cu).

In each case, compounds **4**−**10** were isolated as solid samples in moderate to good yields. They exhibit a good solubility in common polar organic solvents. The ionic derivatives **6**, **7**, and **10** are, however, insoluble in diethylether, hydrocarbons, and water. They are thermally very stable with temperatures of decomposition rising from 203 °C (**6**) to 312 °C (**10**). This feature may deserve some interest, as a good thermal stability is required for incorporation of chromophores into polymers matrix with high glass transition temperature (Tg), an important prerequisite for various practical uses.[4b,42]

Composition and identity of the new complexes were deduced from elemental analysis, multidimensional NMR spectroscopic methods, mass spectrometry, and absorption spectroscopy (see Experimental Section). Additionally, the crystal and molecular structures of **4** and **8** were determined by single crystal X-ray diffraction analysis (see below). We were unable to obtain single crystals of trinuclear species, but their molecular structures are readily assigned from spectroscopic data. Mass spectra of measured compounds show the presence of peaks of molecular ion $[M]^+$ with 100% intensity, corresponding to the neutral species or to the cationic fragment, in the case of the trinuclear salts **6**, **7**, and **10**. For all these peaks, the envelope of the isotopic pattern was in good agreement with the simulated ones.

The IR spectral data of the six Schiff base complexes **4**−**7**, **9**, and **10** support the coordination of the tetradentate acyclic ligand (ONNO) to the central 3d metal ions by means of nitrogen atoms of the 1,2-diamino bridge and two oxygen atoms of the ferrocenylacetonic and salicylidene fragments.[22] For instance, the ν(C═N) stretching vibration of the organometallic Schiff base ligand **8** (1639 cm^{-1}) is shifted by 20 cm^{-1} toward lower frequencies upon complex formation, revealing coordination of the imine nitrogen atom to the nickel ion in **9**. Moreover, the spectra of the ionic derivatives **6**, **7**, and **10** exhibit a very strong absorption band at about 840 cm^{-1} and a medium intensity band at 557 cm^{-1}, assigned to the $\nu(PF_6)$ and δ(P−F) modes of the PF_6^- anion, respectively, testifying to the complexation of the Cp^*Ru^+ arenophile. The characteristic ν(O−H) stretching bands at frequencies higher than 3100 cm^{-1} of the 5-OH substituent is also observed in the IR spectra of **8**−**10**.

The ^1H and $^{13}C\{^1H\}$ NMR data for the diamagnetic derivatives (**4**, **6**, **8**, **9**, and **10**) are reported in the Experimental Section with the atom labeling scheme in Chart 2. The presence of the imine proton N═CH between 7.68 and 9.12 ppm confirms the assembly of quadridentate Schiff base ligands. In each compound, the ferrocenyl enamidoketone fragment is clearly identified by the three sharp singlets in the chemical shift ranges 1.95−2.50, 4.08−4.24, and 5.32−5.87 ppm (integral ratio 3:5:1), attributed to the methyl, the unsubstituted cyclopentadienyl ring, and the pseudoaromatic methine protons, respectively. The *o*-phenylene and ethylene bridge protons show up as four and two (or four in the case of **10**) distincts resonances, respectively, confirming the unsymmetrical nature of the complexes. Moreover, the salicylidene ring protons of **4** and **6** give again rise to four distinct resonances, while for **8**−**10** a typical doublet, double doublet, doublet multiplicity pattern assigned to H-3, H-4, and H-6 protons (integral ratio 1:1:1), respectively, stands for the signature of the 5-hydroxosalicylidene ring. Interestingly, the substituted cyclopentadienyl ring H_α and H_β protons which appear as two triplets for the dinuclear complexes **4** and **9**, give rise to four resonances (integral signal ratio 1:1:1:1) on passing to their respective trinuclear counterparts **6** and **10** (see Supporting Information, Figure S1). This feature, we have previously reported for trinuclear relatives, arises from sterically hindered rotation of the ferrocenyl moiety about the C_{ipso}-C(O)- bond, further to complexation of the salicylidene ring by the bulky arenophile Cp^*Ru^+.[22,43] Note that this splitting does not occur in the more flexible dinuclear compound **3** (see Supporting Information). As expected, spectra of both **6** and **10** show sharp singlets integrating for 15 H at 2.10 ppm for the pentamethylcyclopentadienyl protons and the characteristic upfield shift ($0.75 < \Delta\delta < 1.31$ ppm) of the salicylidene ring proton signals, thus firmly establishing the η^6-coordination of the Cp^*Ru^+ arenophile.[44] All these assignments are confirmed by ^{13}C NMR data which fully support the unsymmetrical nature of the compounds (see Experimental Section and Supporting Information).

In the case of the two paramagnetic copper(II) compounds **5** and **7**, the solution effective magnetic moments were determined by Evans' NMR method,[45] at 297 K in CD_3COCD_3, to be 1.98 μ_B and 2.05 μ_B, respectively. These values, in close agreement with, albeit slightly greater than, the spin-only magnetic moment value for a d^9 Cu^{II} ion ($S = 1/2$, 1.73 μ_B), are in the observed range 1.80−2.00 μ_B and consistent with the expected monomeric structure of the two complexes.[14b,22a,46]

(43) Such a splitting has also been observed in sterically constrained Diferrocenylbispyran systems: Ba, F.; Cabon, N.; Robin-Le Guen, F.; Le Poul, P.; Le Poul, N.; Le Mest, Y.; Golhen, S.; Caro, B. *Organometallics* **2008**, *27*, 6396.

(44) Hubig, S. M.; Lindeman, S. V.; Kochi, J. K. *Coord. Chem. Rev.* **2000**, *200*−*202*, 831.

(45) (a) Evans, D. F. *J. Chem. Soc.* **1959**, 2003. (b) Crawford, T. H.; Swanson, J. *J. Chem. Educ.* **1971**, *48*, 382. (c) Schubert, E. M. *J. Chem. Educ.* **1992**, *69*, 62.

(46) Cotton, F. A.; Wilkinson, G.; Murillo, C. A.; Bochmann, M. *Advanced Inorganic Chemistry*, 6th ed.; Wiley-Interscience: New York, 1999; p 867.

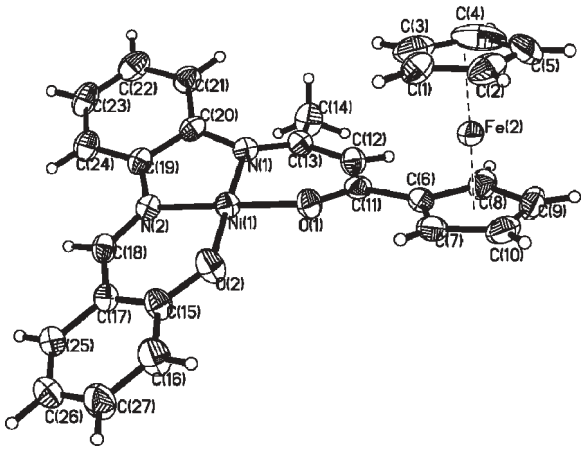

Figure 1. ORTEP diagram for compound **4** showing the atom numbering scheme. Displacement ellipsoids are at the 40% probability level. Selected bond distances (Å) and angles (deg): Ni(1)−O(1) 1.842(2), Ni(1)−O(2) 1.849(2), Ni(1)−N(1) 1.868(3), Ni(1)−N(2) 1.848(3), O(1)−C(11) 1.283(4), O(2)−C(27) 1.304(4), N(1)−C(13) 1.325(4), N(2)−C(21) 1.307(4); O(1)−Ni(1)−N(1) 94.85(12), O(1)−Ni(1)−O(2) 83.82(11), O(2)−Ni(1)−N(2) 95.16(12), N(1)−Ni(1)−N(2) 86.17(13).

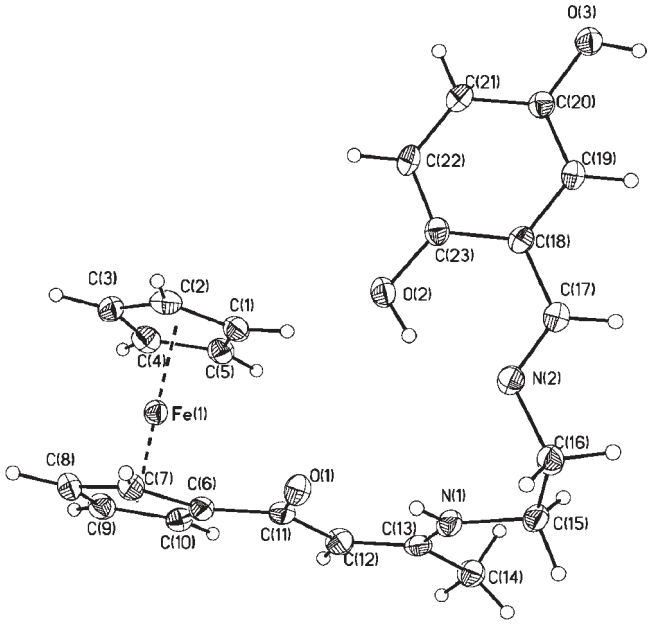

Figure 2. ORTEP diagram for compound **8** showing the atom numbering scheme. Displacement ellipsoids are at the 40% probability level. Selected bond distances (Å) and angles (deg): O(1)−C(11) 1.271(3), O(2)−C(23) 1.363(3), N(1)−C(13) 1.323(3), N(2)−C(17) 1.282(3), N(1)−C(15) 1.457(3), N(2)−C(16) 1.459(3); O(1)−C(11)−C(12) 122.4(2), O(2)−C(23)−C(18) 122.3(2), C(13)−N(1)−C(15) 127.2(2), C(16)−N(1)−C(17) 119.5(2).

X-ray Crystallographic Studies. Figures 1 and 2 show the structures of the binuclear derivative **4** and of the metalloligand **8**, respectively, with selected bond distances and angles given in the captions (see Supporting Information, Tables S1 and S2, respectively, for more complete data). Compounds **4** and **8** crystallize in the monoclinic space groups $P2_1/c$ and $P2_1/n$, respectively, with in each case four molecules present in the asymmetric unit. Complex **4** consists of a ferrocenyl fragment linked to an unsymmetrical Schiff base complex of nickel(II), whereas in compound **8** the ferrocenyl moiety is attached to a potential tetradentate acyclic ligand. The two C_5-ligands in the same ferrocenyl group are essentially parallel, with the ring centroid-iron-ring centroid angles of 178.36° for **4** and 177.72° for **8**. For the two molecules, the ring centroid-iron distances of 1.637, 1.645 Å and 1.644, 1.651 Å for the ring with and without the side chain, respectively, indicate that there is a Fe^{II} oxidation state in the metallocenes.[47]

Organometallic-inorganic hybrid **4** can be described as a classical Werner-type coordination compound where a dianionic unsymmetrical quadridentate Schiff base ligand formally binds nickel(II) ion through two nitrogen atoms (amido and imine) and two oxygen atoms (ketone and phenolato). This tetradentate binding leads to the formation of a six-, five-, six-membered chelate ring arrangement around the central metal ion which is essentially square planar with the nitrogen and oxygen atoms occupying mutually *trans* positions. This is reflected in the two diagonal O−Ni−N angles of 178.95(12) and 178.34(12)°, barely deviating from linearity. As a result, the deviation of the nickel atom away from the plane defined by the chelating hetero atoms [O(1)−N(1)−N(2)−O(2)] is only 0.006 Å. As the NMR spectrum was free from line broadening it can be assumed that the deviation from square planar is not significant. As usually observed for this family of complexes,[22,48] the bond lengths associated with the nickel atom are virtually equal within the error of the measurement (see caption of Figure 1 and Supporting Information, Table S1).

The two external chelate rings [O(1) to N(1)] and [O(2) to N(2)] are planar. The former is almost coplanar with the substituted cyclopentadienyl ring of the ferrocenyl unit (dihedral angles = 8.73°), whereas the dihedral angles between the plane of the latter and that of the salicylidene C_6-ring is 1.79°. These two subunits are held together by the five-membered ring defined by the nickel atom, the two nitrogens, and their two linked *ortho* carbons of the *o*-phenylene ring; the N−C−C−N torsion angle is of 4.66°. Most notably, the chelating Schiff base unit is actually quite strongly bowed with an angle between the two central carbon atoms, C(12) and C(22), of the 6-membered chelate rings and the Ni atom of 159.5°. This may be a consequence of the rigidity brought about by the *o*-phenylene bridge as the corresponding angle of the more flexible ethylene-bridged counterpart is almost linear (177.9°).[22a] Finally, the bond lengths of the chelate rings (see Supporting Information, Table S1) are very similar to those measured previously in $Ni^{II}(N_2O_2)$ derivatives, independent of the ligand.[12a,c,22,48] Overall, the structural data reported here are indicative of substantial π delocalization

(47) For a reference gathering a large number of interatomic and metal-ligand distances obtained from the Cambridge Crystallographic Data Base Centre, see: Orpen, A. G.; Brammer, L.; Allen, F. H.; Kennard, D.; Watson, D. G.; Taylor, R. *J. Chem. Soc., Dalton Trans.* **1989**, S1.

(48) For recent structural characterizations of $Ni(N_2O_2)$ Schiff base compounds, see, for example: (a) Trujillo, A.; Fuentealba, M.; Carrillo, D.; Manzur, C.; Hamon, J.-R. *J. Organomet. Chem.* **2009**, *694*, 1435. (b) Rotthaus, O.; Jarjayes, O.; Philouze, C.; Pérez Del Valle, C.; Thomas, F. *Dalton Trans.* **2009**, 1792. (c) Maity, D.; Chattopadhyay, S.; Ghosh, A.; Drew, M. G. B.; Mukhopadhyay, G. *Polyhedron* **2009**, *28*, 812. (d) Wu, J.-C.; Liu, S.-X.; Keene, T. D.; Neels, A.; Mereacre, V.; Powell, A. K.; Decurtins, S. *Inorg. Chem.* **2008**, *47*, 3452. (e) Maity, D.; Mukherjee, P.; Ghosh, A.; Drew, M. G. B.; Mukhopadhyay, G. *Inorg. Chim. Acta* **2008**, *361*, 1515.

Table 2. Formal Electrode Potentials and Peak-to-Peak Separations for the Fe^{II}/Fe^{III} Redox Processes Exhibited by the Schiff Base Complexes **4**−**10**[a]

compound	$E_{1/2}$/V (ΔE_p/mV)	compound	$E_{1/2}$/V (ΔE_p/mV)
4[b]	0.130 (170)	**6**[b]	0.140 (120)
5[b]	0.110 (95)	**7**[b]	0.120 (150)
8[c]	0.090 (95)		
9[c]	0.050 (60)	**10**[c]	0.070 (66)

[a] Recorded in dichloromethane at 293 K, 0.1 M *n*-$Bu_4N^+PF_6^-$ as supporting electrolyte; all potentials are quoted vs $Cp_2Fe^{0/+}$, scan rate = 0.1 V s^{-1}. [b] Vitreous carbon working electrode. [c] Platinum disk working electrode.

of the electron density through these rings, thus allowing electronic communication between both metal centers.

The single-crystal X-ray diffraction study of the potentially tetradentate metalloligand **8** confirms both the monomeric nature of the compound and the Z-s-Z conformational form[49] adopted by the ferrocenyl enaminone part of the molecule (Figure 2), as it was previously found for its precursor **2**.[22b] The structure reveals that the plane made by the enaminone side chain is virtually coplanar with the substituted cyclopentadienyl ring (dihedral angle = 9.06°), and partial delocalization of the heteroconjugated [O−C−C−C−N] frameworks (see Supporting Information, Table S2) with a dihedral angle between the respective planes of 60.76°. Moreover, the structure of **8** is stabilized by a network of intra- and intermolecular hydrogen bonds through N−H, two O−H and C═O groups (see Supporting Information, Figure S2 and Table S3).

Electrochemistry. Electrochemical potentials also offer information regarding donor−acceptor interactions. Compounds **4**−**10** were studied using CV in CH_2Cl_2/0.1 M *n*-Bu_4NPF_6; potentials are summarized in Table 2 and representative voltammograms are shown in the Supporting Information (Figure S3). Each complex displays one chemically reversible oxidation process with current ratio i_{pa}/i_{pc} equal to unity, assignable as a monoelectronic transition at the ferrocenyl moiety. These redox events arise from the oxidation of the monosubstituted ferrocene unit and correspond to the generation at the electrode of the respective mono- and dicationic Fe^{III} species. Interestingly, the potential of each compound under investigation is shifted to more oxidizing potential than that of free ferrocene; the $E_{1/2}$ values of the trinuclear derivatives **6**, **7**, and **10** are slightly more shifted to the anodic regime than those of their binuclear counterparts **4**, **5**, and **9**, respectively (Table 2). These differences between the $E_{1/2}$ values for the three pairs **4**/**6**, **5**/**7**, and **9**/**10** are indeed small (10−20 mV), falling almost within the experimental errors of CV measurements. One must, therefore, be cautious in interpreting those data but the observed anodic shift tendency is real and expected on passing from the neutral species to its cationic counterpart. Moreover, the present data are in accordance with our previous observations within this family of bi- and trinuclear macroacyclic unsymmetrical Schiff base complexes.[22] However, this increased difficulty of oxidation of the Fe^{II} center features the electron withdrawing ability of both the neutral and the cationic Schiff base side chain. The experimental results for the **8**−**10** series are also supported by DFT calculations (vide infra).

Table 3. UV-vis Data for the Schiff Base Complexes **4**−**10**

compd	λ/nm (Log ε) (CH_2Cl_2)	λ/nm (Log ε) (DMSO)	solv. shift (cm^{-1})
4	252 (4.82)		
	304 (4.35)	276 (4.41)	−3340
	376 (4.56)	376 (3.39)	0
	407 (3.51)	404 (3.52)	−182
	440 (3.60)	425 (3.89)	−802
	587 (3.16)	577 (3.11)	−292
5	290 (3.2)	290 (3.2)	0
	389 (3.3)	390 (3.3)	−66
	440 (2.3)	445 (2.5)	+255
	445 (2.8)	449 (2.7)	+200
6	229 (4.47)		
	319 (4.12)	309 (4.06)	−1014
	395 (4.10)	398 (3.97)	+191
	454 (3.34)	451 (3.20)	−147
	490 (3.48)	484 (3.50)	−253
	612 (3.25)	590 (3.10)	−609
7	274 (3.84)		
	368 (3.57)	384 (3.69)	+1130
	474 (3.08)	452 (3.29)	−1030
8	237 (3.3)	244 (4.3)	+1210
	342 (4.6)	343 (3.5)	+85
	459 (3.3)	455 (3.2)	−192
9	245 (3.9)		
	310 (3.4)	319 (4.1)	+910
	390 (2.8)	396 (3.4)	+388
	434 (3.4)	426 (3.4)	−433
	471 (3.1)	460 (3.6)	−508
10	287 (4.2)	288 (4.1)	+121
	369 (3.9)	364 (3.7)	−372
	387 (3.5)	388 (3.4)	+67
	455 (3.1)	416 (3.4)	−2060

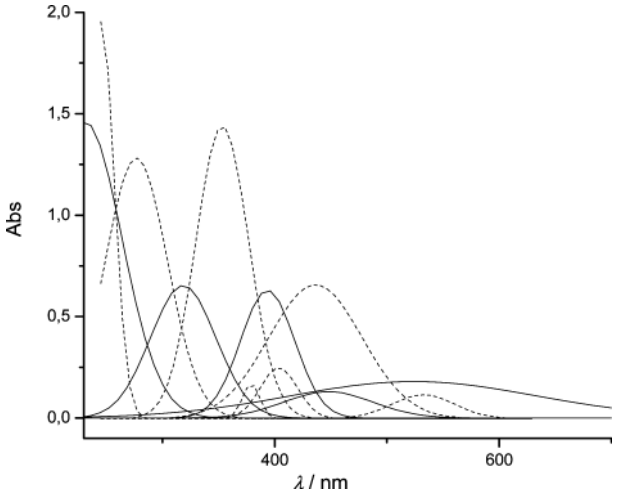

Figure 3. Deconvoluted UV−vis spectra of **4** (dashed line) and **6** (solid line) showing the bathochromic shift of the absorption peaks upon complexation of the arenophile.

Electronic Absorption Spectra. The electronic absorption spectra in the UV−visible region were measured in CH_2Cl_2 and DMSO for the Schiff base complexes **4**−**10** and are reported in Table 3. The spectra are rather similar and consist of two intense broad absorption bands (Supporting Information, Figure S4), which strongly suggest that the electronic properties of these systems are dominated by the donor−acceptor substituted organometallic

(49) (a) Greenhill, J. V. *Chem. Soc. Rev.* **1977**, *6*, 277. (b) Tietze, L. F.; Bergmann, A.; Brill, G.; Brüggemann, K.; Hartël, U.; Voss, E. *Chem. Ber.* **1989**, *122*, 83. (c) Shi, Y. C.; Yang, H. M.; Shen, W. B.; Yan, C. G.; Hu, X. Y. *Polyhedron* **2004**, *23*, 15. (d) Shi, Y. C.; Yang, H. M.; Shen, W. B.; Yan, C. G.; Hu, X. Y. *Polyhedron* **2004**, *23*, 1541.

Chart 3

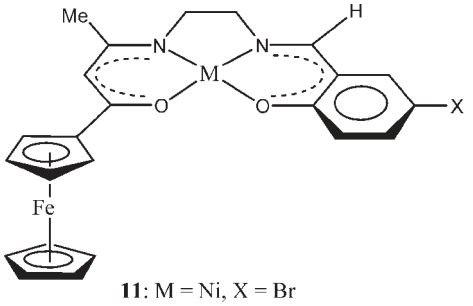

11: M = Ni, X = Br
12: M = Cu, X = Br
15: M = Ni, X = $OCH_2CH{=}CH_2$

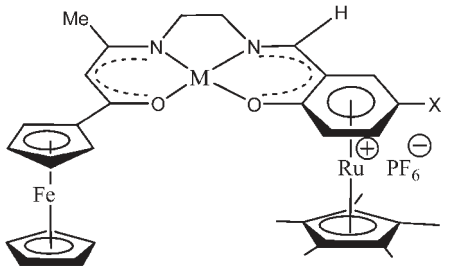

13: M = Ni, X = Br
14: M = Cu, X = Br

Table 4. Experimental Values of the Dipolar First Hyperpolarizability β for Schiff Base Derivatives **4**–**7**, **10**, and Related Complexes[a]

compd	(10^{-30} esu)[b]	compd	(10^{-30} esu)[c]
4	250	**6**	235
5	212	**7**	237
15[d]	230	**10**	247
11[d]	226	**13**[d]	241
12[d]	206	**14**[d]	215

[a] Obtained by means of HLS measurements. [b] As 10^{-2} M $CHCl_3$ solutions. [c] As 10^{-2} M DMF solutions. [d] Structures depicted in Chart 3.

chromophore. Upon deconvolutions of the spectra with Gaussian curves, these two absorption bands give rise to a set of three to six transitions. The origin of the high-energy absorption bands in the range 230–395 nm, is assumed to be intraligand $\pi-\pi^*$ transitions, and the low-energy absorption bands in the 400–600 nm region presumably involve metal-to-ligand and ligand-to-metal CT.[50,51] In addition, the CT band is influenced by the presence of the Cp^*Ru^+ arenophile, which produces a bathochromic shift (Figure 3). This behavior suggests a ligand-to-metal CT (LMCT) nature of this transition. All those major features of the experimental spectra are well reproduced by the calculated transitions (see the Theoretical Section below). On the other hand, upon moving from CH_2Cl_2 (ε = 8.90) to the more polar solvent DMSO (ε = 47.6), the low energy structures exhibit a moderate hypsochromic shift (Supporting Information, Figure S4, Table 3), characteristic of a dipole moment change between the ground and the excited state, and indicative of CT character. This behavior (blue shift in solvents of higher polarity), which seems to be a trend observed in donor–acceptor salicylaldiminato Schiff base complexes,[11] is usually associated with reduction in the dipole moment upon electronic excitation, and therefore potential NLO capabilities (see below).

Quadratic NLO Studies. The quadratic nonlinearities of the new Schiff base complexes **4**–**7** and **10**, two pairs of bi- and trinuclear relatives (**11**/**13**[22b] and **12**/**14**)[52] and the functionalized allyloxo derivative **15**[48a] (see formulas in Chart 3) have been determined at the 1.91 μm incident wavelength using the HLS technique (see Experimental Section). The experimental values of the multipolar first hyperpolarizability β values are presented in Table 4. For solubility reason, the HLS measurements were carried out in chloroform for the neutral binuclear species and in DMF for the trinuclear salts. Comparison of NLO responses must be done with great care owing to the relative error (about 10%) in the determination of the hyperpolarizabilities and the different techniques and experimental conditions used. Although data collected in Table 4 indicate a NLO response for this family of chromophores comparable to that previously calculated and observed for salicylaldiminato Ni^{II} and Cu^{II} derivatives,[7a,11] they do not allow the establishment of any clear structure–activity relationships as they are close to the experimental errors. Nevertheless, a slight enhancement of β values can be noted on passing from the neutral binuclear complexes to the trinuclear salts and upon substitution of nickel(II) for copper(II). However, the measurements of the second-order nonlinearity for both the metalloligand **8** and its trinuclear counterpart **10** have been carried out under the same conditions in DMF and showed an enhancement of the NLO response, with the hyperpolarizabilities of the complex equal to 1.5 times that of the free ligand ($\beta = 155 \times 10^{-30}$ esu). Complexation of **8** by Ni^{II} ion is accompanied by the formation of a geometrically constrained acentric planar structure which is expected to enhance the bridge conjugation and, hence, the nonlinearity. Therefore, this 1.5-fold enhancement arises presumably from a combination of geometric and electronic effects.

Theoretical Investigations. To get a better understanding of the structure and properties of compounds **4**–**10**, we have investigated the electronic structure of their simplified models in which the methyl group on the N_2O_2 Schiff base core has been replaced by a hydrogen atom. These models, labeled **4′**-**10′**, are depicted in Chart 4. Their optimized geometries are shown in Figure S5 (see Supporting Information) and some of their relevant computed data is given in Table 5. When available, metrical data obtained from X-ray structure determination of related complexes are provided in parentheses. A good agreement between the computed and experimental values can be noted. In the case of the trinuclear complexes, two conformations, namely, *anti* and *syn*, are

(50) (a) Fuentealba, M.; Garland, M. T.; Carrillo, D.; Manzur, C.; Hamon, J.-R.; Saillard, J.-Y. *Dalton Trans.* **2008**, 77. (b) Houjou, H.; Motoyama, T.; Araki, K. *Eur. J. Inorg. Chem.* **2009**, 533. (c) Bosnich, B. *J. Am. Chem. Soc.* **1968**, *90*, 627.

(51) Lever, A. B. P. *Inorganic Electronic Spectroscopy*; 2nd edn., Elsevier: New York, 1984.

(52) Trujillo, A.; Carrillo, D.; Manzur, C.; Hamon, J.-R. work in progress.

(53) Albright, T. A.; Burdett, J. K.; Whangbo, M. H. *Orbitals Interactions in Chemistry*; Wiley: New York, 1985.

Chart 4

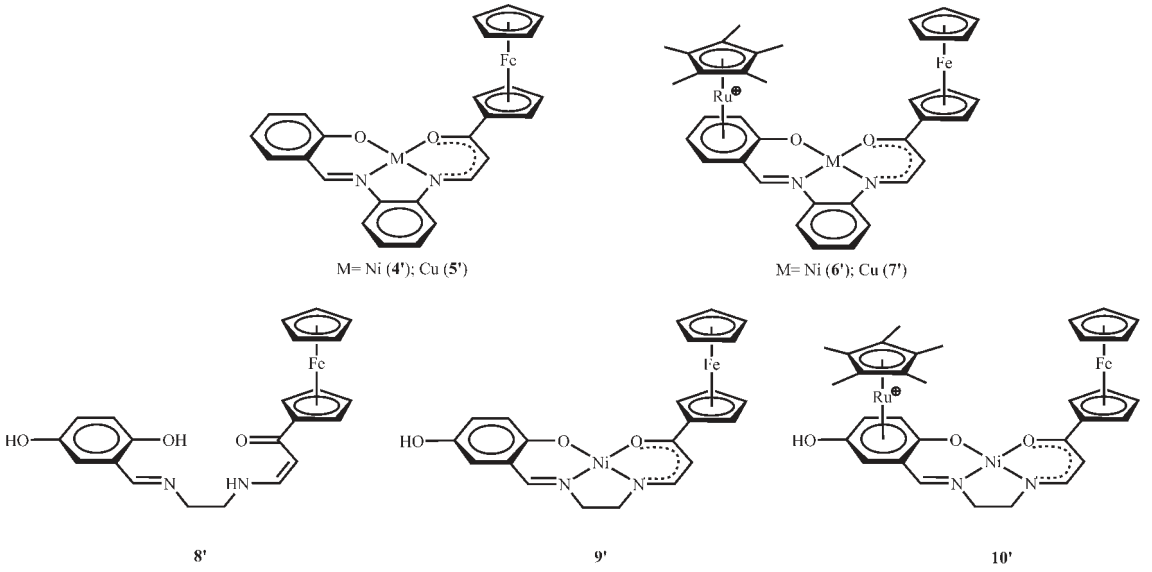

Table 5. Major Metrical Data (in Å) for the Optimized Geometries of **4′**−**10′**[a]

	4′	**5′**	**6′**	**7′**	**8′**	**9′**[b]	**10′**[c]
M−N(1)	1.887 (1.868)	1.973	1.875	1.962		1.869 (1.856)	1.866 (1.834)
M−O(1)	1.904 (1.842)	1.976	1.882	1.969		1.901 (1.846)	1.873 (1.825)
M−N(2)	1.889 (1.848)	1.987	1.892	2.025		1.862 (1.851)	1.871 (1.881)
M−O(2)	1.886 (1.849)	1.950	1.901	1.977		1.894 (1.844)	1.921 (1.852)
C−N(1)	1.335 (1.325)	1.334	1.342	1.339	1.346 (1.323)	1.323 (1.315)	1.327 (1.328)
C−O(1)	1.291 (1.283)	1.287	1.294	1.289	1.267 (1.271)	1.295 (1.298)	1.302 (1.244)
C−N(2)	1.318 (1.307)	1.313	1.311	1.302	1.294 (1.282)	1.310 (1.302)	1.301 (1.249)
C−O(2)	1.304 (1.304)	1.301	1.290	1.288	1.348 (1.363)	1.308 (1.322)	1.290 (1.309)
Fe−Cp_{CNT}	1.697 (1.645)	1.695	1.700	1.701	1.693 (1.651)	1.694 (1.648)	1.697 (1.630)
Fe−Cp'_{CNT}	1.690 (1.637)	1.685	1.688	1.698	1.686 (1.644)	1.685 (1.642)	1.686 (1.639)
Ru−Cp^*_{CNT}			1.878	1.879			1.883 (1.793)
Ru−Sal_{CNT}			1.852	1.848			1.847 (1.732)

[a]Abbreviations: Cp = η^5-C_5H_5, Cp′ = η^5-C_5H_4, Cp* = η^5-C_5Me_5, Sal = salicylidene ring, CNT = centroid. Experimental values are in parentheses. For atom numbering scheme see Figure 1. [b] Experimental values taken from ref 48a. [c] Experimental values taken from ref 22a.

possible, depending if the organometallic moieties lie on opposite sides or on the same side of the planar Schiff base skeleton, respectively. It should be noted that all the known experimental structures of complexes discussed in this paper exhibit the *syn* configuration.[22,50a] Even so, geometry optimization for models **6′** and **10′** was performed for both conformations. Their difference in energy was found to be less than 1 kcal/mol indicating that both isomers are isoenergetic at the considered level of theory. Consistently, their electronic structures were found to be very similar. These results prompted us to carry out the geometry optimization of the odd-electron model **7′** in the *syn* conformation only. All the results discussed here correspond to those obtained in the *syn* conformation.

The molecular orbital diagrams of the computed models are shown in Figure 4 in which all the highest occupied molecular orbital (HOMO) energies have been set to zero for sake of comparison. For graphical simplicity, the diagrams of the odd-electron species **5′** and **7′** correspond to spin-restricted calculations, whereas all their other computed data given in this paper correspond to spin-unrestricted calculations (see Computational Details). Related computed pertinent numerical data are gathered in Table 6. We start the MO analysis with the **8**−**10** series which offers the possibility to analyze the changes when the metal nuclearity varies from one to three. In the case of the mononuclear model **8′** the Fe^{II} center lies in a pseudo-octahedral environment and therefore its five d-type orbitals split into three occupied nonbonding orbitals so-called "t_{2g}" lying far below two antibonding ones so-called "e_g*".[53] Two π* orbitals of the Schiff base ligand constitute the lowest vacant levels. Thus, the frontier orbitals of **8′** follow the order "t_{2g}"-Fe (occupied) < π^*_{CN} (LUMO) < π^*_{CO} < "e_g*"-Fe. When replacing two ligand protons in **8′** by a Ni(II) atom to generate the dinuclear model **9′**, two levels of large nickel character appear in the HOMO−LUMO area. The HOMO is now a nickel d_π-type orbital (33%) mixed in an antibonding way with some occupied π ligand levels (48%) and with some iron admixture (12%) (Table 6). The lowest unoccupied molecular orbital (LUMO) is a $d_{x^2-y^2}$ orbital mixed in a strongly antibonding way with the ligand σ-type lone pairs. Adding a Cp^*Ru^+ moiety to **9′** to make **10′**, results in significant changes in the frontier MO diagram, not only because supplementary orbitals are added but also because of the effect of the positive charge on the ruthenium center. This charge effect is to stabilize the orbitals to an extent related to their degree of localization close to the ruthenium center. Thus, the orbitals having significant ligand participation are parti-

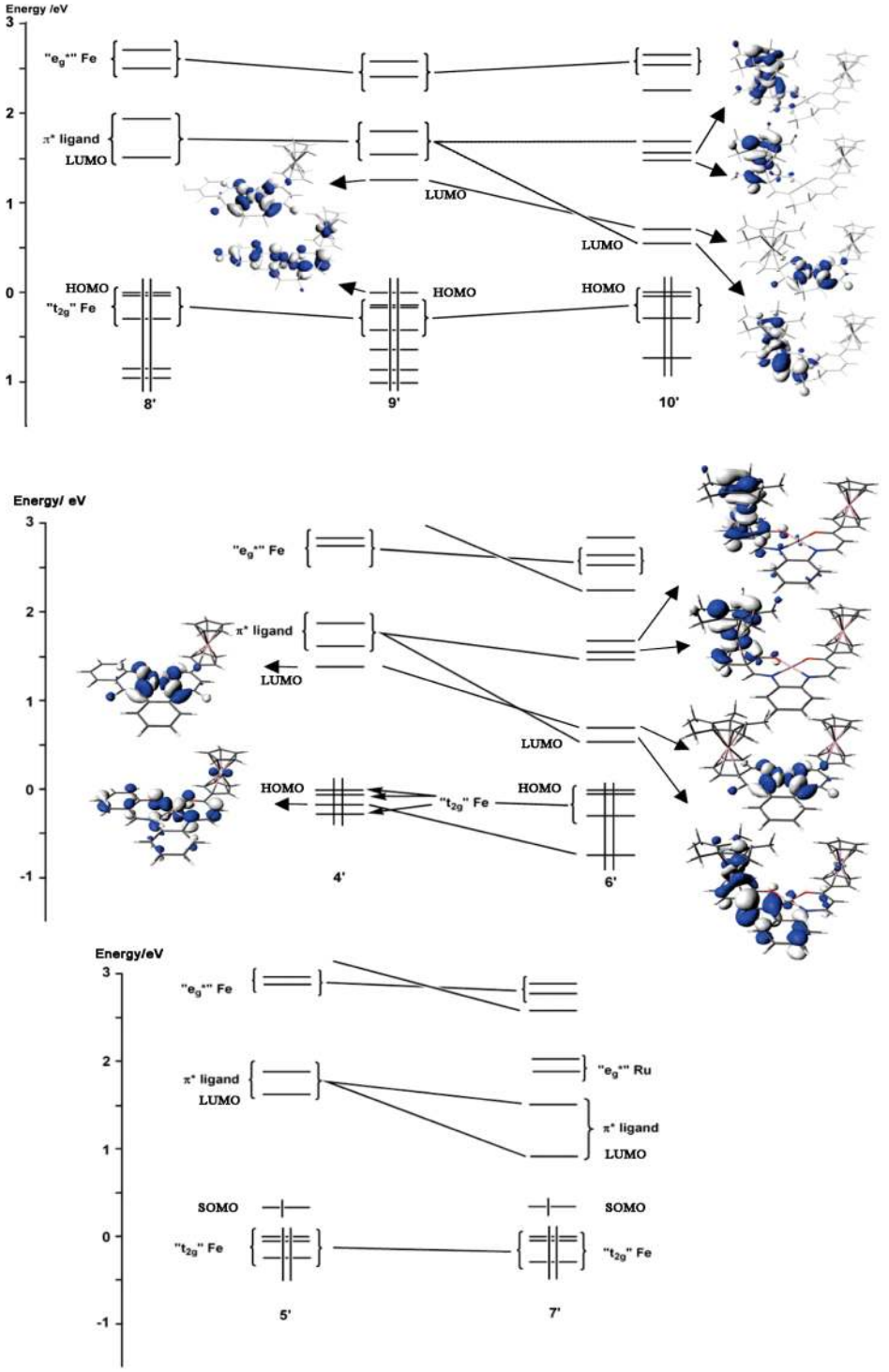

Figure 4. Computed MO diagrams of **4′**−**10′** models. The HOMO energies have been arbitrarily set to zero for clarity.

cularly stabilized. This is the case for most of the lowest unoccupied orbitals. The result is a significant reduction of the HOMO−LUMO gap when going from **9′** (1.3 eV) to **10′** (0.6 eV). The LUMO is now a π* ligand orbital with some Ru participation (Table 6). The Ni-centered LUMO+1 corresponds to the LUMO of **9′**. The "e_g*"-Ru orbitals are the next highest levels, the "e_g*"-Fe orbitals lying now far above. The three highest occupied MOs of **10′** are the "t_{2g}"-Fe orbitals, whereas its HOMO+4 corresponds to the HOMO of **9′**. The "t_{2g}"-Ru levels lie farther below. The level ordering of **4′** is similar to that of **9′**, except that the d_π-Ni/ π−ligand combination is now the HOMO+3. Similarly, the MO diagram of **6′** resembles that of its trinuclear relative **10′**. With one electron more than **4′** and **6′**, their copper analogues **5′** and **7′** exhibit qualitatively similar MO diagrams (see Figure 4), except that the extra electron lies in a Cu($d_{x^2-y^2}$)-ligand antibonding orbital which corresponds to the LUMO of **4′** and **6′**, respectively.

To obtain a rationalization of the experimental redox properties of the compound series **8**−**10** we explored the changes in the electronic structure of the mono-oxidized

Table 6. Relevant Energetic and Electronic Data Computed for Complexes **4′**−**10′**

	4′	**5′**	**6′**	**7′**	**8′**	**9′**	**10′**
HOMO−LUMO gap (eV)	1.4		0.6		1.6	1.3	0.6
			Mulliken Charges (Spin Density)				
Fe	0.05	0.05(0.00)	0.02	0.02(0.07)	0.05	0.06	0.03
M	0.57	0.69(0.47)	0.57	0.68(0.45)		0.57	0.59
Ru			0.77	0.79(0.00)			0.79
Ligand	−0.62	−0.74(0.53)	−0.36	−0.49(0.48)	−0.05	−0.63	−0.41
			Orbital Contributions HOMO/LUMO				
%Fe	75/0		82/0		81/0	12/0	82/0
%M	2/56		0/3		−/−	33/55	0/5
%Ru	−/−		0/13		−/−	−/−	0/16
%Ligand	13/35		12/76		13/96	48/37	12/71

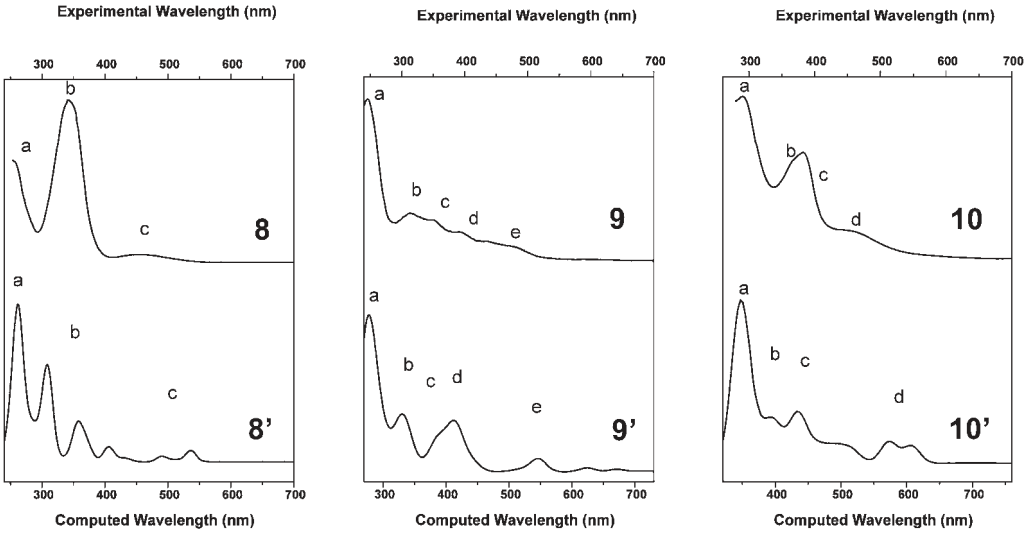

Figure 5. Experimental (top) and calculated (bottom) electronic spectra for complexes **8′**−**10′**.

complexes $\mathbf{8'}^{+}$, $\mathbf{9'}^{+}$, and $\mathbf{10'}^{+}$. In the mono oxidized complex $\mathbf{8'}^{+}$, the computed spin densities exhibit values close to 1 (0.92) on the iron atom. Moreover, the computed Mulliken charges shows the localization of the positive charge over the ferrocenyl group. As expected, the one-electron oxidation of **8′** corresponds to the oxidation of the iron center in the ferrocenyl fragment. On the other hand, the oxidation of **9′** corresponds to the removal of one electron from his HOMO, resulting in a spin density distributed on the iron atom (0.50), the ligand (0.34), and the nickel atom (0.16). The ionization potentials (IP) of the processes $\mathbf{8'} \rightarrow \mathbf{8'}^{+}$ (6.12 eV) and $\mathbf{9'} \rightarrow \mathbf{9'}^{+}$ (5.81 eV) are consistent with the experimental oxidation potentials observed in Table 2. Finally, the oxidation of **10′** involves an energy level that is mainly based on the iron atom of the ferrocenyl fragment (88%) and the rest on the ligand (12%). The ionization potential value (8.23 eV) is much larger than the IP value computed for **8′** and **9′**. This is because in the case of the cation **10′**, the calculations do not account for the existence of interacting counterions which are likely to modify significantly its orbital energies.

We complemented our theoretical investigation by analyzing the electronic spectra of complexes **8**−**10** through TDDFT calculations. Figure 5 shows the experimental (top) and theoretical (bottom) spectra of **8**−**10** and **8′**−**10′**, respectively. The theoretical spectra have been simulated from the computed TDDFT transition wavelengths and oscillator strengths. A good agreement between them is observed. The major features of the experimental spectra are satisfactorily well reproduced by the simulated spectra. This allowed us to propose a band indexation shown in Figure 5. The analysis of the major components of the various transitions associated with the computed bands led to the identification of the corresponding CTs. For compound **8′**, most of the electronic transitions are $\pi-\pi^*$ intraligand CT (ILCT), with some metal-to-ligand $Fe(t_{2g}) \rightarrow \pi^*$ and ligand-to-metal $\pi \rightarrow Fe(e_g^*)$ CTs (MLCT and LMCT, respectively). For the dinuclear complex **9′** the band of lower energy (e) is dominated by $Fe(t_{2g}) \rightarrow \pi^*$ and $Ni \rightarrow \pi^*$ transfer (MLCT). The adjacent band (d) is mainly $\pi \rightarrow$ Ni LMCT with some nickel $d \rightarrow d$ character. The middle band (c) is associated with $Ni \rightarrow Fe(e_g^*)$ d-d CT. No significant participation of iron $d \rightarrow d$ CT was found in the investigated energy range for models **8′** and **9′**. Finally, in the cationic compound **10′** we observed in the high-energy bands (a-b) ruthenium d-d transitions and $Ni \rightarrow Ru(e_g^*)$ d-d transitions. The low-energy band (c) exhibits iron d-d transitions and $Ru(t_{2g}) \rightarrow \pi^*$ MLCT transitions. The rest of the electronic transitions are similar to those described for compounds **8′** and **9′**. The lowest energy band (d) is for the most part due to $Fe(t_{2g}) \rightarrow \pi^*$ MLCT transition. The general tendency of the computed long wavelength bands to be red-shifted relative to experiment (see Figure 5) is

related to the well-known underestimation by TDDFT of low-lying excitation energies associated with significant charge-transfer.[54] On the other hand, the corresponding blue-shift observed for some of the short wavelength bands (in particular band b) is related to the antibonding nature of most of the involved excited states whose energy is systematically overestimated by TDDFT which does not account for electronic relaxation effects.[54d]

Conclusion

Two series of robust neutral binuclear and their corresponding cationic trinuclear organometallic donor−acceptor substituted unsymmetrical Salophen- and salen-type complexes have been synthesized and fully characterized, and their electrochemical, linear, and second order NLO properties have been thoroughly investigated. All the organometallic-inorganic D-π-A conjugated molecules investigated in this work contain ferrocene and M[ONNO] units (M = Ni^{II}, Cu^{II}); the salicylidene ring of the acyclic tetradentate Schiff base core being π-coordinated to the 12-electron cationic arenophile Cp^*Ru^+ in the trinuclear series. The studies of single crystal X-ray diffraction analysis shows for the bimetallic Fe−Ni derivative **4** the coplanarity of Ni[ONNO] core inserted into a bowed unsymmetrical Schiff base framework (C(12)−Ni(1)−C(22) ca. 160°), whereas for the mononuclear metalloligand **8** the two heteroconjugated [O−C−C−C-N] frameworks make a dihedral angle of 60.76°. Theoretical calculations have also been performed using DFT and TDDFT, allowing a detailed understanding of the electronic structure and absorption spectra of the complexes. The DFT calculated energy levels of frontier orbitals and large spin density of iron centers for the **8′**−**10′** series are in accordance with the experimental electrochemical results. As well, a fairly good correlation of the measured and calculated (TDDFT) absorption maxima has been observed for most of complexes, and the ILCT and the MLCT contributions in the overall band have been determined. Finally, HLS measurements showed that all the compounds exhibited a second-order nonlinear response, the hyperpolarizability (β) value increasing with the nuclearity of the complexes, and that the donor−acceptor substituents dominate the nonlinearity. Immobilization of such unsymmetrical redox and NLO active Schiff base systems onto resin and solid materials is currently the subject of further investigations.

Acknowledgment. We thank P. Hamon (Rennes) for measuring the magnetic susceptibility moments of **5** and **7**. Thanks are also addressed to Drs. S. Sinbandhit and P. Jehan (CRMPO, Rennes) for assistance with the 2D NMR and HRMS experiments, respectively. Computing facilities were provided by the IDRIS-CNRS Center at Orsay (France). This research has been performed as part of the Chilean-French Joint Laboratory for Inorganic Functional Materials (LIA MIF N° 836). Financial support from the Fondo Nacional de Desarrollo Científico y Tecnológico (FONDECYT, Chile), Grant 1040851 (C.M. and D.C.), the ECOS-SUD (France) - CONICYT (Chile) agreement no. C05E03, the Vicerrectoría de Investigación y Estudios Avanzados, Pontificia Universidad Católica de Valparaíso, Chile (C.M. and D.C.), the University of Rennes 1, the CNRS and the Institut Universitaire de France (J.-Y.S.) is gratefully acknowledged. A.T. thanks the CONICYT (Chile) for support of a graduate fellowship.

Supporting Information Available: Synthesis and spectroscopic characterization of **3**, discussion of the ^{13}C NMR spectra, details on the X-ray crystallographic study of **4** and **8**, tables of bond distances and angles for **4** and **8**, hydrogen bonding pattern of **8**, ^1H NMR spectra of **4** and **6**, CVs of **4**−**7**, electronic absorption spectra of **6**, **7**, and **10**, optimized geometries of **4′**−**10′**, and tables of Computed Cartesian Coordinates for **4′**−**10′**. Crystallographic files in CIF format for the two reported X-ray crystal structures. This material is available free of charge via the Internet at http://pubs.acs.org.

(54) (a) Neugebauer, J.; Gritsenko, O.; Baerends, E. J. *J. Chem. Phys.* **2004**, *124*, 21402. (b) Peach, M. J. G.; Benfield, P.; Helgaker, T.; Tozer, D. J. *J. Chem. Phys.* **2008**, *128*, 4418. (c) Ziegler, T.; Seth, M.; Krykunov, M.; Autschbach, J.; Wang, F. *J. Mol. Struc: THEOCHEM* **2009**, *914*, 106. (d) Neese, F. *Coord. Chem. Rev.* **2009**, *253*, 526.